acetylcholinesterase inhibitor. Jpn J Pharmacol 2002;89:7-20

25. Okamura N, Funaki Y, Tashiro M, et al. In vivo visualization of donepezil binding in the brain of patients with Alzheimer's disease. Br J Clin Pharmacol 2008;65:472-9
26. Shinotoh H, Aotsuka A, Fukushi K, et al. Effect of donepezil on brain acetylcholinesterase activity in patients with AD measured by PET. Neurology 2001;56:408-10
27. Villemagne VL, Musachio JL, Scheffel U. Neuronal nicotinic receptors: pharmacology and therapeutic opportunities. New York: John Wiley & Sons, 1998
28. Nordberg A, Hartvig P, Lilja A, et al. Nicotine receptors in the brain of patients with Alzheimer's disease. Studies with 11C-nicotine and positron emission tomography. Acta Radiol Suppl 1991;376:165-6
29. Horti AG, Villemagne VL. The quest for Eldorado: development of radioligands for in vivo imaging of nicotinic acetylcholine receptors in human brain. Curr Pharm Des 2006;12:3877-900
30. Ellis JR, Villemagne VL, Nathan PJ, et al. Relationship between nicotinic receptors and cognitive function in early Alzheimer's disease: a 2-[18F]fluoro-A-85380 PET study. Neurobiol Learn Mem 2008;90:404-12
31. Koch HJ, Haas S, Jurgens T. On the physiological relevance of muscarinic acetylcholine receptors in Alzheimer's disease. Curr Med Chem 2005;12:2915-21
32. Wess J, Eglen RM, Gautam D. Muscarinic acetylcholine receptors: mutant mice provide new insights for drug development. Nat Rev Drug Discov 2007;6:721-33
33. Eckelman WC. Imaging of muscarinic receptors in the central nervous system. Curr Pharm Des 2006;12:3901-13
34. Donnemiller E, Heilmann J, Wenning GK, et al. Brain perfusion scintigraphy with 99mTc-HMPAO or 99mTc-ECD and 123I-beta-CIT single-photon emission tomography in dementia of the Alzheimer type and diffuse Lewy body disease. Eur J Nucl Med 1997;24:320-5
35. O'Brien JT, Colloby S, Fenwick J, et al. Dopamine transporter loss visualized with FP-CIT SPECT in the differential diagnosis of dementia with Lewy bodies. Arch Neurol 2004;61:919-25
36. Hu XS, Okamura N, Arai H, et al. 18F-fluorodopa PET study of striatal dopamine uptake in the diagnosis of dementia with Lewy bodies. Neurology 2000;55:1575-7
37. Tatsch K. Imaging of the dopaminergic system in differential diagnosis of dementia. Eur J Nucl Med Mol Imaging 2008;35(Suppl 1):S51-7
38. Watanabe H, Ieda T, Katayama T, et al. Cardiac 123I-meta-iodobenzylguanidine (MIBG) uptake in dementia with Lewy bodies: comparison with Alzheimer's disease. J Neurol Neurosurg Psychiatry 2001;70:781-3
39. Yoshita M, Taki J, Yokoyama K, et al. Value of 123I-MIBG radioactivity in the differential diagnosis of DLB from AD. Neurology 2006;66:1850-4
40. Venneti S, Lopresti BJ, Wiley CA. The peripheral benzodiazepine receptor (Translocator protein 18kDa) in microglia: from pathology to imaging. Prog Neurobiol 2006;80:308-22
41. Cagnin A, Brooks DJ, Kennedy AM, et al. In-vivo measurement of activated microglia in dementia. Lancet 2001;358:461-7
42. Edison P, Archer HA, Gerhard A, et al. Microglia, amyloid, and cognition in Alzheimer's disease: An [11C](R) PK11195-PET and [11C]PIB-PET study. Neurobiol Dis 2008;32:412-9
43. Okello A, Edison P, Archer HA, et al. Microglial activation and amyloid deposition in mild cognitive impairment: a PET study. Neurology 2009;72:56-62
44. Wiley CA, Lopresti BJ, Venneti S, et al. Carbon 11-labeled Pittsburgh Compound B and carbon 11-labeled (R)-PK11195 positron emission tomographic imaging in Alzheimer disease. Arch Neurol 2009;66:60-7
45. Doorduin J, de Vries EF, Dierckx RA, et al. PET imaging of the peripheral benzodiazepine receptor: monitoring disease progression and therapy response in neurodegenerative disorders. Curr Pharm Des 2008;14:3297-315
46. Vickers JC, Dickson TC, Adlard PA, et al. The cause of neuronal degeneration in Alzheimer's disease. Prog Neurobiol 2000;60:139-65
47. Hardy J, Selkoe DJ. The amyloid hypothesis of Alzheimer's disease: progress and problems on the road to therapeutics. Science 2002;297:353-6
48. Price JL, Morris JC. Tangles and plaques in nondemented aging and 'preclinical' Alzheimer's disease. Ann Neurol 1999;45:358-68
49. Masters CL, Beyreuther K. Alzheimer's centennial legacy: prospects for rational therapeutic intervention targeting the Abeta amyloid pathway. Brain 2006;129:2823-39
50. Villemagne VL, Ng S, Cappai R, et al. La Lunga Attesa: towards a molecular approach to neuroimaging and therapeutics in Alzheimer's disease. Neuroradiol J 2006;19:51-75
51. Klunk WE, Debnath ML, Pettegrew JW. Chrysamine-G binding to Alzheimer and control brain: autopsy study of a new amyloid probe. Neurobiol Aging 1995;16:541-8
52. Skovronsky DM, Zhang B, Kung MP, et al. In vivo detection of amyloid plaques in a mouse model of Alzheimer's disease. Proc Natl Acad Sci USA 2000;97:7609-14
53. Zhuang ZP, Kung MP, Hou C, et al. Radioiodinated styrylbenzenes and thioflavins as probes for amyloid aggregates. J Med Chem 2001;44:1905-14
54. Link CD, Johnson CJ, Fonte V, et al. Visualization of fibrillar amyloid deposits in living, transgenic Caenorhabditis elegans animals using the sensitive amyloid dye, X-34. Neurobiol Aging 2001;22:217-26
55. Klunk WE, Bacskai BJ, Mathis CA, et al. Imaging Aß plaques in living transgenic mice with multiphoton microscopy and methoxy-X04, a systemically administered Congo red derivative. J Neuropath Exp Neurol 2002;61:797-805
56. Agdeppa ED, Kepe V, Liu J, et al. Binding characteristics of radiofluorinated 6-dialkylamino-2-naphthylethylidene derivatives as positron emission tomography imaging probes for beta-amyloid plaques in Alzheimer's disease. J Neurosci 2001;21:RC189
57. Barrio JR, Kepe V, Satyamurthy N, et al. Amyloid and tau imaging, neuronal losses and function in mild cognitive impairment. J Nutr Health Aging 2008;12:61S-5S
58. Small GW, Kepe V, Ercoli LM, et al. PET of brain amyloid and tau in mild cognitive impairment. N Engl J Med 2006;355:2652-63

59. Tolboom N, Yaqub M, van der Flier WM, et al. Detection of Alzheimer pathology in vivo using both 11C-PIB and 18F-FDDNP PET. J Nucl Med 2009;50:191-7

60. Shin J, Lee SY, Kim SH, et al. Multitracer PET imaging of amyloid plaques and neurofibrillary tangles in Alzheimer's disease. Neuroimage 2008;43:236-44

61. Klunk WE, Wang Y, Huang GF, et al. The binding of 2-(4'-methylaminophenyl) benzothiazole to postmortem brain homogenates is dominated by the amyloid component. J Neurosci 2003;23:2086-92

62. Mathis CA, Wang Y, Holt DP, et al. Synthesis and evaluation of 11C-labeled 6-substituted 2-arylbenzothiazoles as amyloid imaging agents. J Med Chem 2003;46:2740-54

63. Lockhart A, Lamb JR, Osredkar T, et al. PIB is a non-specific imaging marker of amyloid-beta (Aβ) peptide-related cerebral amyloidosis. Brain 2007;130:2607-15

64. Maeda J, Ji B, Irie T, et al. Longitudinal, quantitative assessment of amyloid, neuroinflammation, and anti-amyloid treatment in a living mouse model of Alzheimer's disease enabled by positron emission tomography. J Neurosci 2007;27:10957-68

65. Harigaya Y, Saido TC, Eckman CB, et al. Amyloid beta protein starting pyroglutamate at position 3 is a major component of the amyloid deposits in the Alzheimer's disease brain. Biochem Biophys Res Commun 2000;276:422-7

66. Fodero-Tavoletti MT, Smith DP, et al. In vitro characterization of Pittsburgh compound-B binding to Lewy bodies. J Neurosci 2007;27:10365-71

67. Price JC, Klunk WE, Lopresti BJ, et al. Kinetic modeling of amyloid binding in humans using PET imaging and Pittsburgh Compound-B. J Cereb Blood Flow Metab 2005;25:1528-47

68. Lopresti BJ, Klunk WE, Mathis CA, et al. Simplified quantification of Pittsburgh Compound B amyloid imaging PET studies: a comparative analysis. J Nucl Med 2005;46:1959-72

69. McNamee RL, Yee SH, Price JC, et al. Consideration of optimal time window for Pittsburgh compound B PET summed uptake measurements. J Nucl Med 2009;50:348-55

70. Fazio F, Perani D. Importance of partial-volume correction in brain PET studies. J Nucl Med 2000;41:1849-50

71. Lowe J, Kemp BJ, Jack CR Jr, et al. Comparison of 18F-FDG and PiB PET in cognitive impairment. J Nucl Med 2009;50:878-886

72. Klunk WE, Engler H, Nordberg A, et al. Imaging brain amyloid in Alzheimer's disease with Pittsburgh Compound-B. Ann Neurol 2004;55:306-19

73. Rowe CC, Ng S, Ackermann U, et al. Imaging beta-amyloid burden in aging and dementia. Neurology 2007;68:1718-25

74. Bacskai BJ, Frosch MP, Freeman SH, et al. Molecular imaging with Pittsburgh Compound B confirmed at autopsy: a case report. Arch Neurol 2007;64:431-4

75. Ikonomovic MD, Klunk WE, Abrahamson EE, et al. Post-mortem correlates of in vivo PIB-PET amyloid imaging in a typical case of Alzheimer's disease. Brain 2008;131:1630-45

76. Leinonen V, Alafuzoff I, Aalto S, et al. Assessment of beta-amyloid in a frontal cortical brain biopsy specimen and by positron emission tomography with carbon 11-labeled Pittsburgh Compound B. Arch Neurol 2008;65:1304-9

77. Gomperts SN, Rentz DM, Moran E, et al. Imaging amyloid deposition in Lewy body diseases. Neurology 2008;71:903-10

78. Johnson KA, Gregas M, Becker JA, et al. Imaging of amyloid burden and distribution in cerebral amyloid angiopathy. Ann Neurol 2007;62:229-34

79. Archer HA, Edison P, Brooks DJ, et al. Amyloid load and cerebral atrophy in Alzheimer's disease: an 11C-PIB positron emission tomography study. Ann Neurol 2006;60:145-7

80. Fagan AM, Mintun MA, Mach RH, et al. Inverse relation between in vivo amyloid imaging load and cerebrospinal fluid Abeta(42) in humans. Ann Neurol 2006;59:512-9

81. Buckner RL, Snyder AZ, Shannon BJ, et al. Molecular, structural, and functional characterization of Alzheimer's disease: evidence for a relationship between default activity, amyloid, and memory. J Neurosci 2005;25:7709-17

82. Nelissen N, Vandenbulcke M, Fannes K, et al. Abeta amyloid deposition in the language system and how the brain responds. Brain 2007;130:2055-69

83. Mintun MA, Larossa GN, Sheline YI, et al. [11C]PIB in a nondemented population: potential antecedent marker of Alzheimer disease. Neurology 2006;67:446-52

84. Villemagne VL, Pike KE, Darby D, et al. Abeta deposits in older non-demented individuals with cognitive decline are indicative of preclinical Alzheimer's disease. Neuropsychologia 2008;46:1688-97

85. Fripp J, Bourgeat P, Acosta O, et al. Appearance modeling of 11C PiB PET images: characterizing amyloid deposition in Alzheimer's disease, mild cognitive impairment and healthy aging. Neuroimage 2008;43:430-9

86. Forsberg A, Engler H, Almkvist O, et al. PET imaging of amyloid deposition in patients with mild cognitive impairment. Neurobiol Aging 2008;29:1456-65

87. Jack CR Jr, Lowe VJ, Senjem ML, et al. 11C PiB and structural MRI provide complementary information in imaging of Alzheimer's disease and amnestic mild cognitive impairment. Brain 2008;131:665-80

88. Engler H, Forsberg A, Almkvist O, et al. Two-year follow-up of amyloid deposition in patients with Alzheimer's disease. Brain 2006;129:2856-66

89. Edison P, Archer HA, Hinz R, et al. Amyloid, hypometabolism, and cognition in Alzheimer disease: an [11C]PIB and [18F]FDG PET study. Neurology 2007;68:501-8

90. Jack CR Jr, Lowe VJ, Weigand SD, et al. Serial PIB and MRI in normal, mild cognitive impairment and Alzheimer's disease: implications for sequence of pathological events in Alzheimer's disease. Brain 2009;132:1355-65

91. Zhuang ZP, Kung MP, Wilson A, et al. Structure-activity relationship of imidazo[1,2-a]pyridines as ligands

for detecting β-amyloid plaques in the brain. J Med Chem 2003;46:237-43

92. Ono M, Wilson A, Nobrega J, et al. 11C-labeled stilbene derivatives as Abeta-aggregate-specific PET imaging agents for Alzheimer's disease. Nucl Med Biol 2003;30:565-71

93. Verhoeff NP, Wilson AA, Takeshita S, et al. In-vivo imaging of Alzheimer disease beta-amyloid with [11C]SB-13 PET. Am J Geriatr Psychiatry 2004;12:584-95

94. Okamura N, Suemoto T, Shimadzu H, et al. Styrylbenzoxazole derivatives for in vivo imaging of amyloid plaques in the brain. J Neurosci 2004;24:2535-41

95. Kudo Y, Okamura N, Furumoto S, et al. 2-(2-[2-Dimethylaminothiazol-5-yl] ethenyl)-6-(2-[fluoro]ethoxy)benzoxazole: a novel PET agent for in vivo detection of dense amyloid plaques in Alzheimer's disease patients. J Nucl Med 2007;48:553-61

96. Rowe CC, Ackerman U, Browne W, et al. Imaging of amyloid beta in Alzheimer's disease with 18F-BAY94-9172, a novel PET tracer: proof of mechanism. Lancet Neurol 2008;7:129-35

97. Okamura N, Suemoto T, Furumoto S, et al. Quinoline and benzimidazole derivatives: candidate probes for in vivo imaging of tau pathology in Alzheimer's disease. J Neurosci 2005;25:10857-62

98. Boxer AL, Rabinovici GD, Kepe V, et al. Amyloid imaging in distinguishing atypical prion disease from Alzheimer disease. Neurology 2007;69:283-90

99. Villemagne VL, McLean CA, Reardon K, et al. 11C-PiB PET studies in typical sporadic Creutzfeldt-Jakob disease. J Neurol Neurosurg Psychiatry 2009: doi:10.1136/jnnp.2008.171496

100. Hintersteiner M, Enz A, Frey P, et al. In vivo detection of amyloid-beta deposits by near-infrared imaging using an oxazine-derivative probe. Nat Biotechnol 2005;23:577-83

Affiliation

Nobuyuki Okamura[1], Michelle T Fodero-Tavoletti[4], Yukitsuka Kudo[1], Christopher C Rowe[2], Shozo Furumoto[5], Hiroyuki Arai[6], Colin L Masters[3], Kazuhiko Yanai[1] & Victor L Villemagne[†2,3] MD,
[†]Author for correspondence
[1]Tohoku University,
Pharmacology,
Sendai, Japan
[2]Center for PET,
Austin Health,
Nuclear Medicine,
Melbourne, Australia
Tel: 61 3 9496 3321; Fax: 61 3 9458 5023;
E-mail: villemagne@petnm.unimelb.edu.au
[3]The Mental Health Research Institute,
Melbourne, Australia
[4]University of Melbourne,
Pathology,
Melbourne, Australia
[5]Tohoku University,
Cyclotron and Radioisotope Center,
Sendai, Japan
[6]Tohoku University,
Institute of Development, Ageing and Cancer,
Sendai, Japan

European Journal of Pharmacology 617 (2009) 54–58

Contents lists available at ScienceDirect

European Journal of Pharmacology

journal homepage: www.elsevier.com/locate/ejphar

Neuropharmacology and Analgesia

In vitro characterisation of BF227 binding to α-synuclein/Lewy bodies

Michelle T. Fodero-Tavoletti [a,b,c], Rachel S. Mulligan [f], Nobuyuki Okamura [e], Shozo Furumoto [d], Christopher C. Rowe [f], Yukitsuka Kudo [d], Colin L. Masters [c], Roberto Cappai [a,b,c], Kazuhiko Yanai [e], Victor L. Villemagne [a,c,f,*]

[a] Department of Pathology, The University of Melbourne, VIC, Australia
[b] Bio21 Molecular and Biotechnology Institute, The University of Melbourne, VIC, Australia
[c] The Mental Health Research Institute of Victoria, Tohoku University, Sendai, Japan
[d] Biomedical Engineering Research Organization, Tohoku University, Sendai, Japan
[e] Department of Pharmacology, Tohoku University, Sendai, Japan
[f] Department of Nuclear Medicine, Austin Health, Centre for PET, VIC, Australia

ARTICLE INFO

Article history:
Received 4 March 2009
Received in revised form 6 June 2009
Accepted 22 June 2009
Available online 1 July 2009

Keywords:
BF227
α-synuclein
Positron emission tomography
Dementia with Lewy bodies
Aβ (amyloid-β)
Imaging

ABSTRACT

Amyloid-β (Aβ) plaques are a pathological hallmark of Alzheimer's disease and a current target for positron emission tomography (PET) imaging agents. Whilst [^{11}C]-PiB is currently the most widely used PET ligand in clinic, a novel family of benzoxazole compounds have shown promise as Aβ imaging agents; particularly BF227. We characterised the in vitro binding of [^{18}F]-BF227 toward α-synuclein to address its selectivity for Aβ pathology, to establish whether [^{18}F]-BF227 binds to α-synuclein/Lewy bodies, in addition to Aβ plaques. In vitro [^{18}F]-BF227 saturation studies were conducted with 200 nM α-synuclein or $A\beta_{1-42}$ fibrils or 100 μg of Alzheimer's disease, pure dementia with Lewy bodies or control brain homogenates. Non-specific binding was established with PiB (1 μM). In vitro binding studies indicated that [^{18}F]-BF227 binds with high affinity to two binding sites on $A\beta_{1-42}$ fibrils (K_{D1} = 1.31 and K_{D2} = 80 nM, respectively) and to one class of binding sites on α-synuclein fibrils (K_D = 9.63nM). [^{18}F]-BF227 bound to Aβ-containing Alzheimer's disease brain (K_D = 25 ± 0.5 nM), but failed to bind to Aβ-free dementia with Lewy bodies or age-matched control homogenates. Moreover, BF227 labelled both Aβ plaques and Lewy bodies in immunohistochemical/fluorescence analysis of human Alzheimer's disease and Parkinson's disease brain sections, respectively. This study suggests that [^{18}F]-BF227 is not Aβ-selective. Evaluation of BF227 as a potential biomarker for Parkinson's disease is warranted.

1. Introduction

Currently, there is no cure for Alzheimer's disease, an age-related neurodegenerative disease, clinically characterised by dementia. The Alzheimer's disease brain is pathologically characterised by the presence of (i) extracellular amyloid plaques comprising amyloid-β (Aβ); (ii) intracellular neurofibrillary tangles composed of hyperphosphorylated tau; (iii) synaptic loss and reactive gliosis; (iv) increased oxidative damage to lipids, proteins and nucleic acids and (v) biometal dyshomeostasis (Goedert and Spillantini, 2006).

Definitive diagnosis of Alzheimer's disease and related dementias still relies upon postmortem examination. As new therapeutic strategies undergo clinical evaluation, considerable effort is now focused on biomarkers for the early and accurate diagnosis of Alzheimer's disease, as well as therapeutic monitoring. Modern molecular imaging procedures such as positron emission tomography (PET), may provide new insight into Alzheimer's disease by non-invasively identifying the underlying pathology of these diseases in the living. Of late, Pittsburgh compound B [PiB] has proven to be a successful biomarker for the in vivo quantitation of Aβ burden (Klunk et al., 2004; Rowe et al., 2007). Nonetheless, its widespread clinical use is impracticable due to the 20-minute decay half-life of carbon-11, limiting its use to centres with an on-site cyclotron. [^{18}F]-FDDNP also highlights Aβ deposits in the human brain; however, FDDNP also binds to neurofibrillary tangles (Agdeppa et al., 2001), as well as PrP^{sc} (Boxer et al., 2007; Bresjanac et al., 2003). Whilst labelling with a longer half-life isotope [^{18}F] proves to be advantageous, FDDNP's lack of selectivity considerably reduces its ability to provide differential diagnosis of neurodegenerative diseases. Hence, the development of a specific

* Corresponding author. Department of Nuclear Medicine, Austin Health, Centre for PET 145 Studley Rd Heidelberg, VIC, 3084 Australia. Tel.: +61 3 9496 3321; fax: +61 3 9458 5023.
E-mail address: villemagne@petnm.unimelb.edu.au (V.L. Villemagne).

0014-2999/$ – see front matter © 2009 Elsevier B.V. All rights reserved.
doi:10.1016/j.ejphar.2009.06.042

and selective [^{18}F]-labelled imaging agent(s) for molecular Aβ imaging is highly desirable to improve diagnostic accuracy and accelerate discovery and monitoring of therapeutics.

Recently, a novel series of benzoxazole compounds have been developed as PET imaging agents; namely BF227 [2-[2-(2-dimethylaminothiazol-5-yl)ethenyl]-6-[2-(fluoro)ethoxy] benzoxazole] has been demonstrated to bind to $A\beta_{1-42}$ fibrils (with low nanomolar affinity) and Aβ plaques in Alzheimer's disease brain sections (Kudo et al., 2007). [^{11}C]-BF227-PET demonstrated retention in cerebral cortices of Alzheimer's disease patients with very little retention in normal patients; suggesting BF227 as a promising PET imaging agent for the in vivo detection of Aβ pathology in Alzheimer's disease patients. Whilst the specificity of BF227 binding to Aβ has been established, there is limited knowledge regarding its selectivity; particularly since Alzheimer's disease has been described as a 'triple brain amyloidosis' (Trojanowski, 2002), comprising Aβ, tau and α-synuclein that when misfolded, comprise the principal components of senile plaques, neurofibrillary tangles and Lewy bodies. Furthermore, the majority of dementia with Lewy bodies cases exhibit extensive cortical Aβ deposition along the pathognomonic Lewy bodies (McKeith et al., 2005). Hence, critical assessment of new radiotracers such as BF227 is warranted to avoid misinterpretation of results and/or incorrect diagnosis. Whilst BF227 binding to neurofibrillary tangles has previously been examined (Kudo et al., 2007), the potential of BF227 binding to α-synuclein has not been assessed. The aim of this study was to test the ability of BF227 to bind/recognise α-synuclein fibrils/Lewy bodies to establish whether [^{18}F]-BF227 is selective for Aβ pathology.

2. Materials and methods

2.1. Materials

All reagents were purchased from Sigma (St. Louis, MO), unless otherwise stated. Human $A\beta_{1-42}$ was purchased from the W. M. Keck Laboratory (Yale University, New Haven, CT).

2.1.1. Tissue collection and characterisation

Brain tissue was collected at autopsy. The sourcing and preparation of the human brain tissue were conducted by the National Neural Tissue Resource Centre. Alzheimer's disease pathological diagnosis was made according to standard NIA-Reagan Institute criteria (1997). Dementia with Lewy bodies cases was diagnosed using consensus guidelines (McKeith et al., 1996) and classified as either dementia with Lewy bodies-Aβ, being subjects with evidence of neuritic plaques and/or cerebral vascular amyloid, as determined by IHC and ELISA, or pure dementia with Lewy bodies (no significant evidence of neuritic plaques and/or cerebral vascular amyloid). Parkinson's disease pathological diagnosis was made following previously described criteria (Braak et al., 2003; Forno, 1996). Determination of age-matched controls cases were also subject to the above criteria. The number of subject cases utilised is indicated in the figure/table texts. Overall, three Alzheimer's disease, three dementia with Lewy bodies-Aβ, one pure Dementia with Lewy bodies, two Parkinson's disease and three age-matched control subjects were utilised in this study.

2.1.2. [^{18}F] labelling of BF227

Unlabelled BF227 and 2-[2-(2-dimethylaminothiazol-5-yl)ethenyl]-6-[2-(tosyloxy)ethoxy] benzoxazole (BF-226; the precursor for [^{18}F]-BF-227) were custom synthesised by Tanabe R&D Service Co. and confirmed for purity by reverse phase high performance liquid chromatography, one dimensional NMR and mass spectrometry. [^{18}F]-BF227 was synthesised by nucleophilic substitution of the tosylate precursor (BF-226) (see below). Following a 10 min reaction at 110°C the crude reaction was partially purified on an activated Sep Pak tC18 cartridge before undergoing semi preparative reverse phase HPLC purification. Standard tC18 Sep-Pak reformulation produced [^{18}F]-BF227 in >95% radiochemical purity. The radiochemical yield was 17% (non decay corrected) and at the end of the synthesis the average specific activity was 1471 mCi/μmol/42 GBq/μmol.

Schematic for the radiosynthesis of [^{18}F]-BF227.

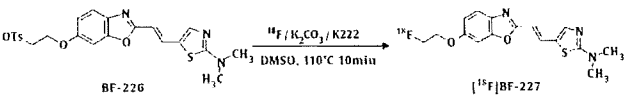

2.1.3. Preparation of amyloid fibrils

Synthetic $A\beta_{1-42}$ was dissolved in 1× PBS pH 7.7 to a final concentration of 200 μM. Recombinant human α-synuclein was expressed and purified as previously described (Cappai et al., 2005) and dissolved in 10 mM phosphate buffer pH 7.4, to a final concentration of 200 μM. These solutions were incubated at 37°C for either 2 days for $A\beta_{1-42}$ or 7 days for α-synuclein, with agitation (220 rpm, Orbital mixer incubator, Ratek). After aggregation, approximately 5% of the protein remained in the supernatant after centrifugation at 12,000×g for 20 minutes. Fibril aggregation was confirmed through ThT fluorescence spectroscopy and electron microscopy.

2.1.4. Preparation of human brain tissue for in vitro binding studies

Grey matter was isolated from the postmortem frontal cortex tissue from the Alzheimer's disease, dementia with Lewy bodies-Aβ, pure dementia with Lewy bodies and age-matched control subjects. Isolated tissue was then homogenised in 1× PBS (without calcium and magnesium), utilising an ultrasonic cell disrupter (2 × 30 s, 24,000 rpm; Virsonic 600, Virtis). Protein concentration was determined using the BCA protein assay (Pierce) and brain tissue homogenates were aliquoted and frozen at −80 °C until used.

2.1.5. In vitro BF227 binding assays

Synthetic $A\beta_{1-42}$ or α-synuclein fibrils (200 nM) were incubated with increasing concentrations of [^{18}F]-BF227 (0.5–200 nM). To account for non-specific binding of [^{18}F]-BF227, the above mentioned reactions were duplicated in the presence of unlabelled 1 μM PiB. The binding reactions were incubated for 1 h at room temperature in 200 μl of assay buffer [PBS, minus Mg^{2+} and Ca^{2+} (JRH Biosciences, Kansas, USA); 0.1% BSA]. Binding of [^{18}F]-BF227 to human brain homogenates was assessed by incubating 100 μg brain homogenate from Alzheimer's disease, pure dementia with Lewy bodies (Aβ-free) and age-matched control subjects with increasing concentrations of [^{18}F]-BF227 (0.1–250nM [^{18}F]-BF227 in the absence or presence of unlabelled PiB (1 μM)), as described above. Bound from free radioactivity was separated by filtration under reduced pressure (MultiScreen HTS Vacuum Manifold; MultiScreen HTS 96-well filtration plates; 0.65 μm, Millipore). Filters were washed three times with 200 μl assay buffer and incubated overnight in 3 ml scintillation fluid. Washed filters were assayed for radioactivity in an automatic gamma counter (Wallac 1480 Wizard 3″; Perkin Elmer). Binding data were analysed with curve fitting software that calculates the K_D and B_{max} using nonlinear regression according to the equation:

$$Y = B_{max} \cdot X$$

$$K_D + X$$

(GraphPad Prism Version 1.0, GraphPad Software, San Diego, CA). All experiments were conducted in triplicate.

2.2. Immunohistochemistry (IHC) and Fluorescence Analysis

Brain tissue from Alzheimer's disease and Parkinson's disease subjects was fixed in 10% formalin/PBS and embedded in paraffin. For immunohistochemistry and fluorescence analysis of BF227, 7 μm serial sections were assessed. Serial sections were deparaffinized and treated with 80% formic acid for 5 min and endogenous peroxidase

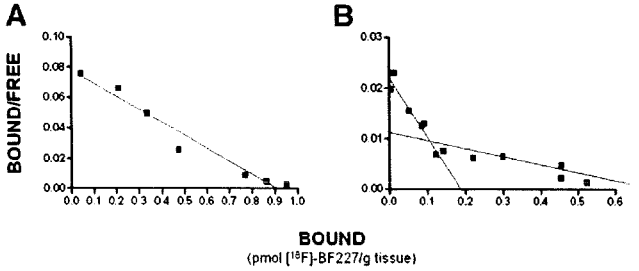

Fig. 1. In vitro binding studies indicate one class of [^{18}F]-BF227 binding sites on α-synuclein fibrils. Scatchard plots of [^{18}F]-BF227 binding to synthetic (A) α-synuclein or (B) $A\beta_{1-42}$ fibrils. (A) Scatchard analysis identified one class of BF227 binding sites on α-synuclein fibrils (K_D of 9.63 nM and B_{max} of 2.76 pmol BF227/nmol α-synuclein). (B) Scatchard analysis identified two classes of BF227 binding sites on $A\beta_{1-42}$; a high affinity binding site with K_D and B_{max} of 1.31 nM and 0.171 pmol BF227/nmol $A\beta_{1-42}$, respectively and a low affinity binding site with K_D and B_{max} of 80.0 nM and 2.96 pmol BF227/nmol $A\beta_{1-42}$, respectively. Binding data were analysed using GraphPad Software (Version 1.0, San Diego, CA). This figure is the average of at least three independent experiments.

activity was blocked utilising 3% hydrogen peroxide. Serial tissue sections were stained in the following order: the first and third sections were immunostained with 97/8 or 1e8 antibodies to identify Lewy bodies or Aβ plaques, respectively and the second section was incubated with BF227. For immunostaining, sections were treated with blocking buffer (20% fetal calf serum, 50 mM Tris–HCl, 175 mM NaCl pH 7.4) before immunostaining with primary antibodies to α-synuclein [97/8; 1:2000 dilution (Culvenor et al., 1999)] or Aβ (1e8; 1:50), for 1 h at room temperature. Visualisation of antibody reactivity was achieved using the LSAB™ kit (labelled streptavidin-biotin, DAKO) and sections were then incubated with hydrogen-peroxidase-diaminobenzidine (H_2O_2–DAB) to visualise the α-synuclein or Aβ-positive deposits. Sections were counterstained with Mayer's hematoxylin. To assess BF227 fluorescence, quenching to minimise autofluorescence was first performed on deparaffinized tissue sections by treatment with 0.25% $KMnO_4$/PBS for 20 min prior to washing (PBS) and incubation with 1% potassium metabisulfite/1% oxalic acid/PBS for 5 min. Following autofluorescence quenching, sections were blocked in 2% BSA/PBS pH 7.0 for 10 min and stained with 100 μM BF227 for 30 min. Washed (PBS) sections were then mounted in non-fluorescent mounting media (DAKO). Epifluorescence images were visualised using a Zeiss microscope (47CFP; filter set 47 (EM BP 436/20, BS FT 455, EM BP480/40). Co-localisation of the BF227 and antibody signals was assessed by overlaying images from each of the stained serial tissue sections.

3. Results

3.1. Characteristics of [^{18}F]-BF227 Binding to Recombinant α-Synuclein and $A\beta_{1-42}$ Fibrils

To investigate the selectivity of BF227, we tested the ability of [^{18}F]-BF227 to bind to synthetic α-synuclein and $A\beta_{1-42}$ fibrils; the major component of Lewy bodies and senile plaques, respectively. The successful formation of fibrils was determined by ThT fluorescence and transmission electron microscopy, prior to conducting the binding assays (data not shown).

Assessment of [^{18}F]-BF227 binding was conducted using equimolar concentrations (200 nM, ~4.0×10^{-11} mol) of either α-synuclein or $A\beta_{1-42}$ fibrils. Scatchard analysis indicated that [^{18}F]-BF227 bound to one site on α-synuclein fibrils with high affinity (K_D 9.63nM; Fig. 1A). In contrast, two classes of binding sites exist for [^{18}F]-BF227 binding to $A\beta_{1-42}$ fibrils (high affinity K_{D1} 1.31 and low affinity K_{D2} 80nM, respectively; Fig. 1B). Despite the two classes of binding sites identified for $A\beta_{1-42}$ fibrils, the total number of binding sites was similar for both α-synuclein (B_{max} 2.76 pmol [^{18}F]-BF227/nmol α-synuclein) and $A\beta_{1-42}$ (B_{max1} 0.171 and B_{max2} 2.96 pmol [^{18}F]-BF227/nmol $A\beta_{1-42}$) fibrils.

3.2. In Vitro [^{18}F]-BF227 Binding Analysis of Human Alzheimer's Disease and Dementia With Lewy Bodies Brain

In previous studies, postmortem human brain homogenates have been extensively utilised to characterise amyloid imaging agents, including PiB (Fodero-Tavoletti et al., 2007; Klunk et al., 1995; Klunk et al., 2003; Klunk et al., 2005; Mathis et al., 2003). To further assess the selectivity of BF227, we compared the in vitro binding properties of [^{18}F]-BF227 to Aβ-containing brain homogenates (Alzheimer's disease) versus Aβ-free (non-detectable levels of Aβ) homogenates (pure dementia with Lewy bodies and age-matched control). Aβ ELISA analysis was utilised to establish the presence/absence (non-detectable levels) of Aβ, prior to conducting binding studies (data not shown). [^{18}F]-BF227 bound with high affinity to Aβ-containing brain homogenates. Scatchard analysis identified one class of binding sites within Alzheimer's disease homogenates with a K_D of 33 ± 4.8 nM and a B_{max} of 9353 pmol/[^{18}F]-BF227/g tissue (Fig. 2A). In contrast, [^{18}F]-BF227 did not bind to the α-synuclein-containing Aβ-free dementia with Lewy bodies (dementia with Lewy bodies-pure; Fig. 2B) or the Aβ-and α-synuclein-free age-matched control subjects (Fig. 2C).

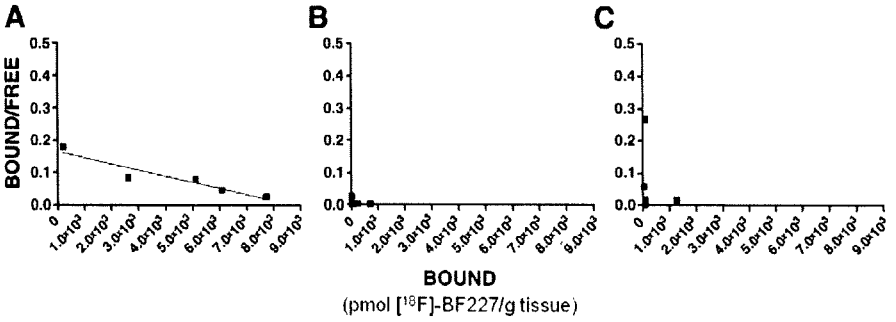

Fig. 2. In vitro binding studies demonstrate that [^{18}F]-BF227 fails to bind to pure dementia with Lewy bodies brain homogenate. Scatchard plots of [^{18}F]-BF227 binding to (A) AD, (B) age-matched control and (C) pure dementia with Lewy bodies brain homogenates. Scatchard analysis indicated that BF227 binds to Alzheimer's disease (K_D 33 ± 4.8nM, B_{max} 9353 pmol/[^{18}F]-BF227/g tissue). No significant binding of [^{18}F]-BF227/g to pure dementia with Lewy body or age-matched control subjects was observed. Binding data were analysed using GraphPad Software (Version 1.0, San Diego, CA). This figure is the average of at least three independent experiments.

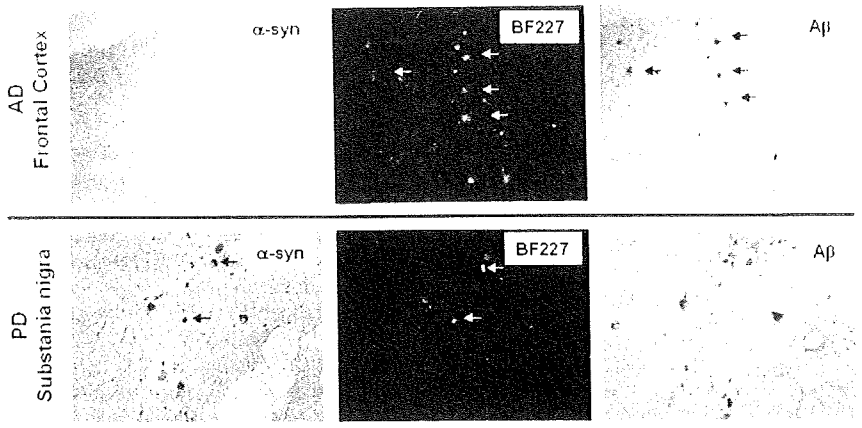

Fig. 3. Immunohistochemistry analysis indicates that BF227 binds specifically to Aβ plaques and not α-synuclein-containing Lewy bodies within the substantia nigra. Microscopy images of three serial sections (7 mm) from the frontal cortex of (A) Alzheimer's disease or (B) substantia nigra Parkinson's disease brain, immunostained with antibodies to α-synuclein (97/8; 1:2000) and Aβ (1E8; 1:50), to identify Lewy bodies and Aβ plaques respectively; or stained with 100 mM BF227. Black arrows indicate the location of Aβ plaques (top panel) and Lewy bodies (bottom panel), as determined by immunohistochemistry. White arrows indicate positive BF227 staining as detected by fluorescence, co-localising with 1E8 immunostaining of Aβ plaques in Alzheimer's disease subjects and Lewy bodies in the substantia nigra of Parkinson's disease subjects. Tissue sections were imaged using a Leica microscope and Axiocam digital camera. Scale bars, 50 mm.

3.3. BF227 and Immunohistochemical Staining of Human Alzheimer's Disease and Parkinson's Disease Subjects

As a qualitative measure of its potential binding to α-synuclein deposits/Lewy bodies by fluorescence microscopy, unlabelled BF227 was used to stain fixed serial sections from the substantia nigra of Parkinson's disease subjects. Staining of the frontal cortex of Alzheimer's disease subjects was also conducted. Parkinson's disease substantia nigra sections were chosen for their rich source of Lewy bodies. BF227 staining of the substantia nigra co-localised with immuno-reactive α-synuclein-containing Lewy bodies (Fig. 3). A comparison of the α-synuclein staining Lewy bodies with BF227 staining suggested that BF227 binds to Lewy bodies as well as Aβ stained plaques.

4. Discussion

The ongoing quest for specific and selective PET imaging agents is imperative for the early diagnosis, treatment, development and monitoring of neurodegenerative diseases, such as Alzheimer's disease. To date, the design and testing of PET imaging candidates have suggested that compounds based on histological dyes whilst specific, are not selective for Aβ pathology. Benzoxazole compounds/derivatives represent a promising new family of imaging agents that may overcome some of the limitations of current PET ligands.

In vitro binding studies indicated that [^{18}F]-BF227 bound significantly to $A\beta_{1-42}$ fibrils; exhibiting two classes of binding sites. Previous studies (Kudo et al., 2007) assessing the binding affinity of BF227 to $A\beta_{1-42}$ fibrils utilised a competition binding assay that was incapable of detecting multiple classes of binding sites. This study is the first to suggest the existence of two binding sites for benzoxazole compounds on $A\beta_{1-42}$ fibrils. Binding of [^{18}F]-BF227 to α-synuclein fibrils was observed only at an equimolar concentration to $A\beta_{1-42}$ fibrils although, with a ~10-fold lower affinity when compared to $A\beta_{1-42}$ fibrils (Fig. 1A). The lower affinity of [^{18}F]-BF227 for synthetic α-synuclein fibrils as compared to $A\beta_{1-42}$ fibrils and the concentration of [^{18}F]-BF227 (~1 nM) typically achieved during PET studies, suggests that the binding of [^{18}F]-BF227 to α-synuclein-containing Lewy bodies should not contribute significantly to the [^{18}F]-BF227-PET signal.

Despite the results obtained for synthetic $A\beta_{1-42}$ fibrils, in vitro studies in brain homogenates failed to show two binding sites. Nevertheless, a high affinity K_D value in the low nanomolar range was observed. This distinction may reflect the fact that Aβ plaques are not only composed of $A\beta_{1-42}$, but also $A\beta_{1-40}$ and other longer or truncated species of Aβ (i.e. $A\beta_{1-39}$ and $A\beta_{1-43}$) within the Alzheimer's disease brain. Despite the binding of [^{18}F]-BF227 to α-synuclein fibrils, no binding of [^{18}F]-BF227 was detected in pure dementia with Lewy bodies homogenates, devoid of Aβ plaques. This observation may indicate that the density of α-synuclein-containing Lewy bodies present in the pure dementia with Lewy bodies homogenates analysed may be low and therefore undetectable by [^{18}F]-BF227. Our previous studies assessing PiB binding to α-synuclein fibrils and pure dementia with Lewy bodies brain homogenates yielded similar results and as remarked there, the concentration of α-synuclein fibrils utilised for the in vitro studies may be physiologically unattainable, explaining the discrepancy between fibril and dementia with Lewy bodies brain homogenate results (Fodero-Tavoletti et al., 2007).

Consistent with previous reports, BF227 staining of Aβ plaques was clearly evident in the Alzheimer's disease brain sections examined. Fluorescence studies also demonstrated that BF227 bound to Lewy bodies, as indicated by the co-localisation of BF227 staining with α-synuclein-positive Lewy bodies (Fig. 3). Noteworthy, the concentration of BF227 used for the fluorescent studies was considerably higher (100 μM) that the low nanomolar concentrations typically achieved during in vivo PET studies (Kudo et al., 2007).

In conclusion this study supports the notion that [^{18}F]-BF227 is not entirely selective for Aβ pathology. Whilst previous PET studies were conducted using the carbon-11 labelled BF227, we anticipate that our results would be applicable to both [^{11}C]- and [^{18}F]-labelled BF227 PET studies, as the chemical nature of BF227 is not altered using either radioisotope. Therefore, taking into consideration the calculated K_D for α-synuclein fibrils and the size and cortical density of Lewy bodies, we speculate that the potential contribution of Lewy bodies to [^{11}C]-BF227-PET retention in the brains of Alzheimer's disease and even dementia with Lewy bodies patients (when assessed), should be considered to be extremely low. Nevertheless, given the high affinity for α-synuclein, added to the high density of Lewy bodies in the substantia nigra of most Parkinson's disease patients, evaluation of BF227 as a Parkinson's disease diagnostic biomarker, does warrant further investigation.

Acknowledgments

The authors would like to thank Prof. Catriona McLean, Fairlie Hinton and Geoff Pavey from the National Neural Tissue Resource

Centre for sourcing and preparation of the human brain tissue. We acknowledge the funding from the National Health and Medical Research Council and Ministry of Health, Labour and Welfare, Japan. RC is an NHMRC Senior Research Fellow.

References

Agdeppa, E.D., Kepe, V., Liu, J., Flores-Torres, S., Satyamurthy, N., Petric, A., Cole, G.M., Small, G.W., Huang, S.C., Barrio, J.R., 2001. Binding characteristics of radiofluorinated 6-dialkylamino-2-naphthylethylidene derivatives as positron emission tomography imaging probes for beta-amyloid plaques in Alzheimer's disease. J. Neurosci. 21, RC189.

Boxer, A.L., Rabinovici, G.D., Kepe, V., Goldman, J., Furst, A.J., Huang, S.C., Baker, S.L., O'Neil, J.P., Chui, H., Geschwind, M.D., Small, G.W., Barrio, J.R., Jagust, W., Miller, B.L., 2007. Amyloid imaging in distinguishing atypical prion disease from Alzheimer disease. Neurology 69, 283–290.

Braak, H., Del Tredici, K., Rub, U., de Vos, R.A., Jansen Steur, E.N., Braak, E., 2003. Staging of brain pathology related to sporadic Parkinson's disease. Neurobiol Aging 24, 197–211.

Bresjanac, M., Smid, L.M., Vovko, T.D., Petric, A., Barrio, J.R., Popovic, M., 2003. Molecular-imaging probe 2-(1-[6-[(2-fluoroethyl)(methyl) amino]-2-naphthyl]ethylidene) malononitrile labels prion plaques in vitro. J Neurosci 23, 8029–8033.

Cappai, R., Leck, S.L., Tew, D.J., Williamson, N.A., Smith, D.P., Galatis, D., Sharples, R.A., Curtain, C.C., Ali, F.E., Cherny, R.A., Culvenor, J.G., Bottomley, S.P., Masters, C.L., Barnham, K.J., Hill, A.F., 2005. Dopamine promotes alpha-synuclein aggregation into SDS-resistant soluble oligomers via a distinct folding pathway. FASEB. J. 19, 1377–1379.

Culvenor, J.G., McLean, C.A., Cutt, S., Campbell, B.C., Maher, F., Jakala, P., Hartmann, T., Beyreuther, K., Masters, C.L., Li, Q.X., 1999. Non-Abeta component of Alzheimer's disease amyloid (NAC) revisited. NAC and alpha-synuclein are not associated with Abeta amyloid. Am. J. Pathol. 155, 1173–1181.

Fodero-Tavoletti, M.T., Smith, D.P., McLean, C.A., Adlard, P.A., Barnham, K.J., Foster, L.E., Leone, L., Perez, K., Cortes, M., Culvenor, J.G., Li, Q.X., Laughton, K.M., Rowe, C.C., Masters, C.L., Cappai, R., Villemagne, V.L., 2007. In vitro characterization of Pittsburgh compound-B binding to Lewy bodies. J. Neurosci. 27, 10365–10371.

Forno, L.S., 1996. Neuropathology of Parkinson's disease. J. Neuropathol. Exp. neurol. 55, 259–272.

Goedert, M., Spillantini, M.G., 2006. A century of Alzheimer's disease. Science. (New. York,. N.Y. 314, 777–781.

Klunk, W.E., Debnath, M.L., Pettegrew, J.W., 1995. Chrysamine-G binding to Alzheimer and control brain: autopsy study of a new amyloid probe. Neurobiol. Aging. 16, 541–548.

Klunk, W.E., Engler, H., Nordberg, A., Bacskai, B.J., Wang, Y., Price, J.C., Bergstrom, M., Hyman, B.T., Langstrom, B., Mathis, C.A., 2003. Imaging the pathology of Alzheimer's disease: amyloid-imaging with positron emission tomography. Neuroimaging Clinics of North America 13, 781–789, ix.

Klunk, W.E., Engler, H., Nordberg, A., Wang, Y., Blomqvist, G., Holt, D.P., Bergstrom, M., Savitcheva, I., Huang, G.F., Estrada, S., Ausen, B., Debnath, M.L., Barletta, J., Price, J.C., Sandell, J., Lopresti, B.J., Wall, A., Koivisto, P., Antoni, G., Mathis, C.A., Langstrom, B., 2004. Imaging brain amyloid in Alzheimer's disease with Pittsburgh compound-B. Ann. Neurol. 55, 306–319.

Klunk, W.E., Lopresti, B.J., Ikonomovic, M.D., Lefterov, I.M., Koldamova, R.P., Abrahamson, E.E., Debnath, M.L., Holt, D.P., Huang, G.F., Shao, L., DeKosky, S.T., Price, J.C., Mathis, C.A., 2005. Binding of the positron emission tomography tracer Pittsburgh compound-B reflects the amount of amyloid-beta in Alzheimer's disease brain but not in transgenic mouse brain. J. Neurosci. 25, 10598–10606.

Kudo, Y., Okamura, N., Furumoto, S., Tashiro, M., Furukawa, K., Maruyama, M., Itoh, M., Iwata, R., Yanai, K., Arai, H., 2007. 2-(2-[2-Dimethylaminothiazol-5-yl]ethenyl)-6-(2-[fluoro]ethoxy)benzoxazole: a novel PET agent for in vivo detection of dense amyloid plaques in Alzheimer's disease patients. J. Nucl. Med. 48, 553–561.

Mathis, C.A., Wang, Y., Holt, D.P., Huang, G.F., Debnath, M.L., Klunk, W.E., 2003. Synthesis and evaluation of 11C-labeled 6-substituted 2-arylbenzothiazoles as amyloid imaging agents. J. Medicinal. Chem. 46, 2740–2754.

McKeith, I.G., Dickson, D.W., Lowe, J., Emre, M., O'Brien, J.T., Feldman, H., Cummings, J., Duda, J.E., Lippa, C., Perry, E.K., Aarsland, D., Arai, H., Ballard, C.G., Boeve, B., Burn, D.J., Costa, D., Del Ser, T., Dubois, B., Galasko, D., Gauthier, S., Goetz, C.G., Gomez-Tortosa, E., Halliday, G., Hansen, L.A., Hardy, J., Iwatsubo, T., Kalaria, R.N., Kaufer, D., Kenny, R.A., Korczyn, A., Kosaka, K., Lee, V.M., Lees, A., Litvan, I., Londos, E., Lopez, O.L., Minoshima, S., Mizuno, Y., Molina, J.A., Mukaetova-Ladinska, E.B., Pasquier, F., Perry, R.H., Schulz, J.B., Trojanowski, J.Q., Yamada, M., 2005. Diagnosis and management of dementia with Lewy bodies: third report of the DLB Consortium. Neurology 65, 1863–1872.

McKeith, I.G., Galasko, D., Kosaka, K., Perry, E.K., Dickson, D.W., Hansen, L.A., Salmon, D.P., Lowe, J., Mirra, S.S., Byrne, E.J., Lennox, G., Quinn, N.P., Edwardson, J.A., Ince, P.G., Bergeron, C., Burns, A., Miller, B.L., Lovestone, S., Collerton, D., Jansen, E.N., Ballard, C., de Vos, R.A., Wilcock, G.K., Jellinger, K.A., Perry, R.H., 1996. Consensus guidelines for the clinical and pathologic diagnosis of dementia with Lewy bodies (DLB): report of the Consortium on DLB International Workshop. Neurology 47, 1113–1124.

Rowe, C.C., Ng, S., Ackermann, U., Gong, S.J., Pike, K., Savage, G., Cowie, T.F., Dickinson, K.L., Maruff, P., Darby, D., Smith, C., Woodward, M., Merory, J., Tochon-Danguy, H., O'Keefe, G., Klunk, W.E., Mathis, C.A., Price, J.C., Masters, C.L., Villemagne, V.L., 2007. Imaging beta-amyloid burden in aging and dementia. Neurology 68, 1718–1725.

Trojanowski, J.Q., 2002. Emerging Alzheimer's disease therapies: focusing on the future. Neurobiol. Aging. 23, 985–990.

Neuropathology 2009; **29**, 536–542 doi:10.1111/j.1440-1789.2009.01007.x

Original Article

Prion protein oligomers in Creutzfeldt-Jakob disease detected by gel-filtration centrifuge columns

Haruhiko Minaki, Kensuke Sasaki, Hiroyuki Honda, Toru Iwaki

Department of Neuropathology, Neurological Institute, Graduate School of Medical Sciences, Kyushu University, Fukuoka, Japan

Prion diseases are diagnosed by the detection of accumulation of abnormal prion protein (PrP) using immunohistochemistry or the detection of protease-resistant abnormal PrP (PrP^{res}). Although the abnormal PrP is neurotoxic by forming aggregates, recent studies suggest that the most infectious units are smaller than the amyloid fibrils. In the present study, we developed a simplified method by applying size-exclusion gel-filtration chromatography to examine PrP oligomers without proteinase K digestion in Creutzfeldt-Jakob disease (CJD) samples, and evaluated the correlation between disease severity and the polymerization degree of PrP. Brain homogenates of human CJD and non-CJD cases were applied to the gel-filtration spin columns, and fractionated PrP molecules in each fraction were detected by western blot. We observed that PrP oligomers could be detected by the simple gel-filtration method and distinctly separated from monomeric cellular PrP (PrP^{c}). PrP oligomers were increased according to the disease severity, accompanied by the depletion of PrP^{c}. The separated PrP oligomers were already protease-resistant in the case with short disease duration. In the cases with quite severe pathology the oligomeric PrP reached a plateau, which may indicate that PrP molecules could mostly develop into amyloid fibrils in the advanced stages. The increase of PrP oligomers correlated with the degree of histopathological changes such as spongiosis and gliosis. The decrease of monomeric PrP^{c} was unexpectedly obvious in the diseased cases. Dynamic changes of both oligomerization of the human PrP and depletion of normal PrP^{c} require further elucidation to develop a greater understanding of the pathogenesis of human prion diseases.

Key words: centrifugation, Creutzfeldt-Jakob disease, gel-filtration chromatography, oligomers, prion proteins.

INTRODUCTION

Prion diseases or transmissible spongiform encephalopathies (TSEs) are a group of fatal neurodegenerative disorders which include scrapie and bovine spongiform encephalopathy (BSE) in animals, and Creutzfeldt-Jakob disease (CJD) in humans. Histopathological changes of the brain are comprised of fine vacuolation, also termed spongiosis, reactive changes of astrocytes, and variable loss of neurons.[1] TSEs are associated with abnormal deposition of prion protein (PrP). The normal, cellular PrP (PrP^{c}) is converted into abnormal PrP (PrP^{sc}) through a process of conformational change where a portion of its α-helical and coil structure is refolded into a β-sheet.[2] PrP^{c} consists of 254 amino acids, and is attached to the cell membrane via a glycosyl-phosphatidylinositol anchor, a membrane glycoprotein expressed in many normal tissues and at higher levels in the brain.[2]

Under physiological conditions, PrP exists as 32–35 kDa protein.[3] PrP^{c} is soluble in detergent and degraded easily by proteases. By contrast, PrP^{sc} is insoluble in detergent and partially resistant to proteases.[3] The method for measurement of PrP^{sc} was fundamentally changed with the development of the conformation-dependent immunoassay (CDI). The CDI uses anti-PrP antibodies that react with an epitope exposed in native PrP^{c}, but which do not bind to native PrP^{sc}, which indicates the conformational change of PrP^{sc}. Studies using the CDI method have demonstrated that most PrP^{sc} is protease sensitive ($sPrP^{sc}$),[4–6] PrP^{sc}

Correspondence: Kensuke Sasaki, MD, Department of Neuropathology, Neurological Institute, Graduate School of Medical Sciences, Kyushu University, 3-1-1 Maidashi, Higashi-ku, Fukuoka 812-8582, Japan. Email: ksasaki@np.med.kyushu-u.ac.jp

Received 17 December 2008; revised 6 January 2009 and accepted 7 January 2009; published online 5 March 2009.

produces neurotoxicity by forming aggregates, and the most infectious units are much smaller than the amyloid fibrils that are often observed in TSE-infected tissues.[7,8] In uninfected human brains, PrP is mainly present in monomeric, dimeric, trimeric, and tetrameric forms, while a small amount of large PrP aggregates are present.[9] By contrast, in prion-infected brains the levels of large PrP aggregates are dramatically increased, although the monomers and small oligomers are still detected.[9,10]

Accumulation of misfolded proteins as insoluble aggregates occurs in several neurodegenerative diseases including dementia with Lewy bodies (DLB),[11] Huntington's disease,[12] Parkinson's disease (PD),[11,12] and Alzheimer's disease (AD),[12–14] and are associated with the formation and accumulation of amyloid fibrils in specific brain areas. In these fibrils and aggregates, the constituent molecules are largely in the β-conformation.[11] Recent studies suggest that the soluble oligomers may be the principal neurotoxic agents. Soluble Aβ oligomers are found in CSF of AD patients; the soluble Aβ content of the human brain is better correlated with the severity of disease than the classical amyloid plaques containing insoluble Aβ deposits,[13] and fibril-free oligomers are toxic to cultured cells and neurons.[15–17] In DLB and PD, α-synuclein accumulates in insoluble inclusions; however, α-synuclein promotes the formation of highly soluble oligomers that precede the insoluble α-synuclein aggregates associated with neurodegeneration.[11]

Prion diseases are conventionally diagnosed by the detection of accumulation of abnormal PrP using immunohistochemistry or the detection of the abnormal PrP with protease resistance (PrP^{res}). Comparison between CDI and western blotting of brain samples from sporadic CJD and variant CJD patients showed that the CDI was 50- to 100-fold more sensitive.[6] It would be highly recommended that the abnormality of PrP molecules should be determined from various perspectives more than protease resistance. In the present study, we tested several spin columns to detect PrP oligomers by a simplified method applying gel filtration chromatography without protease treatment, in CJD patients with various degree of neuropathological change, and evaluated the correlation between the disease severity and the degree of PrP polymerization.

MATERIALS AND METHODS

Brain homogenate preparation

Human brains were collected at autopsy from six sporadic CJD (methionine homozygote at the polymorphic codon 129 and the type 1 PrP^{res}: MM1; one case had an unknown genotype due to the refusal of genetic analyses) and three non-CJD neurological control cases (Table 1). The speci-

Table 1 Details of samples and the grading scores of spongiosis and gliosis

Case no.	Diagnosis	codon129/ PrP^{res} type	Age	Gender	Postmortem time (hours)	Duration of illness (months)	Brain weight (g)	Grading		Oligomer ratio	Monomer ratio
								Spongiosis	Gliosis		
1	sCJD	NA/type1	66	M	NA	2.5	1435	1	1	0.0563	0.1948
2	sCJD	MM/type1	68	F	12.5	2	1260	2	1	0.2606	0.2336
3	sCJD	MM/type1	73	F	19.5	4	1100	3	2	0.473	0.0623
4	sCJD	MM/type1	69	M	8	15	940	4	3	1.1263	0.046
5	sCJD	MM/type1	61	M	3.5	30	745	4	3	0.8908	0.0459
6	sCJD	MM/type1	71	M	NA	10	562	4	3	1.0854	0.069
7	Depression		47	M	4	NA	1490			0.0214	0.8418
8	ALS		68	M	5.5	NA	1470			0.02	0.4787
9	MG		59	M	2	NA	1350			0.0414	0.6879

sCJD, sprodaic CJD; ALS, amyotrophic lateral sclerosis; F, female; M, male; MG, myasthenia gravis; MM, methionine homozygote at prion protein gene codon129 polymorphism; NA, not available/applicable.

mens were stored at −80°C until used. Brain samples of frontal cortex were homogenized to a final concentration of 10% (w/v) in lysis buffer without sodium dodecyl sulfate (SDS) (100 mmol Tris-HCl, 100 mmol NaCl, 10 mmol EDTA, 0.5% Nonidet P-40 (NP-40), 0.5% deoxycholate, pH 7.6)[18] or in lysis buffer with SDS (100 mmol Tris-HCl, 100 mmol NaCl, 10 mmol EDTA, 1% SDS, pH 7.6). Samples were homogenized at 5000 rpm for 30 s in a bead-disrupter homogenizing system (MicroSmash MS-100; Tomy Seiko Co., Ltd., Tokyo, Japan). Homogenates were then clarified by centrifugation at 250 *g* for 5 min and the supernatant was stored at −80°C.

Spin-column gel filtration

The manufacturer's instructions for the columns (BD CHROMA SPIN™-200, 400; Clontech, San Francisco, CA, USA) indicated that the CHROMA SPIN-200 was capable of retrieving nucleic acids more than 350 bases and eliminating proteins smaller than 1000 kDa. The columns were pretreated by centrifuging at 200 *g* for 3 min to discard the storage buffer, and then 500 µL lysis buffer was added and centrifuged at 200 *g* for 3 min twice for the buffer exchange. To determine the protein shift, 0.01% bromophenol blue was added and 75 µL samples were then added to the center of the gel bed. The first centrifugation was made at 120 *g* for 2 min, and the first fraction was collected in the collection tube. Another 40 µL of lysis buffer was added, followed by centrifuging at 120 *g* for 2 min to collect the size-exclusion fractions sequentially. In these operations, we used a centrifuge with a fixed-angle rotor (RA-44; Kubota, Osaka, Japan) or swing-bucket rotor (A-4-62; Eppendorf, Hamburg, Germany). The centrifugal conditions described above were used for the swing-rotor centrifuge, and a milder centrifugation of 120 *g* to prepare the columns and 60 *g* to collect the fractions was used for the fixed angle rotor. Additionally, the fractions and pre-column brain homogenates were treated with 50 µg/mL proteinase-K (PK) to verify whether they contained PrP^{res}.

To evaluate the fractionation profiles we applied western protein standards (MagicMark XP; Invitrogen, Carlsbad, CA, USA) to a spin column. Marker proteins were prepared in sample buffer (NuPAGE LDS sample buffer; Invitrogen) and fractionated by the spin-column gel filtration method. Each fraction was assessed by western blot analysis.

Detection of fractionated prion proteins

Fractionated samples were boiled for 10 min in NuPAGE LDS sample buffer. Proteins were separated by SDS-polyacrylamide gel electrophoresis (SDS-PAGE) in 12% Bis-Tris gels (Invitrogen), and proteins were transferred to polyvinylidene difluoride (PVDF) membranes (Immobilon-P; Millipore, Billerica, MA, USA). The membranes were incubated for 1 h at room temperature with EzBlock (ATTO, Tokyo, Japan) in Tris buffered saline with Tween-20 (TTBS) (10 mmol Tris-HCl, 150 mmol NaCl, 0.05% Tween-20) to block the nonspecific binding of antibodies. Membranes were then incubated for 1 h at room temperature with an anti-prion antibody (mouse monoclonal 3F4, 1:10 000; Signet, Dedham, MA, USA), followed by a peroxidase-conjugated anti-mouse IgG secondary antibody (AP192P, 1:20 000; Chemicon, Temecula, CA, USA). Immunoreaction was visualized using ECL plus Western Blotting Detection System (GE Healthcare; Chalfont St. Giles, Buckinghamshire, UK).

Histopathological grading

The spongiform change and gliosis in the frontal cortex adjacent to the sampling site for brain homogenate preparation for each case were evaluated with HE staining and GFAP immunostaining. The grading criteria of the spongiosis were: 0, none; 1, mild (scattered or focal state); 2, moderate (patchy or laminar state); 3, severe (spread to the whole cortex); and 4, (rarefaction, i.e. status spongiosus). The grading criteria of the gliosis were: 0, none; 1, mild (slightly increased number of astrocytes); 2, moderate (prominent astrocytic cell processes); and 3, severe (numerous hypertrophic astrocytes).

RESULTS

Results from the fractionated molecular weight marker suggested that fractions two to four contained protein molecules of at least 220 kDa or more (Fig. 1). Fraction one consisted mostly of void volume, and was thus unsuitable

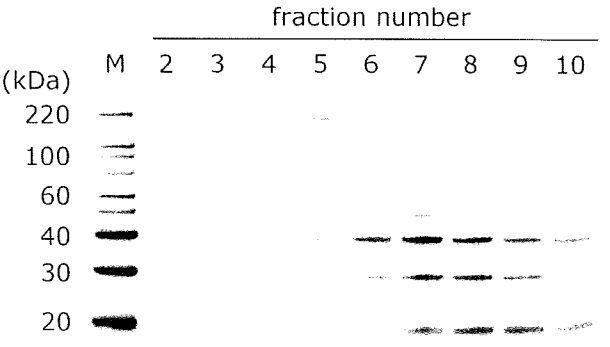

Fig. 1 Western blot analysis for the fractionated molecular markers (MagicMark XP, lane M). Fractions two to four consisted of molecules greater than 220 kDa. Fractions six to nine consisted of molecules of 20–40 kDa.

for assessment. It is estimated that monomeric PrP (size approximately 32–35 kDa) should be mainly collected in fractions six to eight. The experiment with the fixed-angle centrifuge showed a similar fraction pattern as that with the swing-bucket rotor (data not shown).

Proteins were not well separated by CHROMA SPIN-400, which had a pore size larger than CHROMA SPIN-200, particularly in the late-phase fractions (data not shown). Potentially, the gels with the large pores may be too tender to maintain their filtration capacity under the centrifugal conditions used in the present study. Some non-CJD homogenates in the lysis buffer with 0.5% NP-40 and 0.5% deoxycholate showed insoluble PrP aggregates in the peak fractions four to six (Fig. 2a). Therefore, we added 1% SDS in lysis buffer so that most of the PrP molecules were solubilized and detected in fractions six to eight (Fig. 2b). In human CJD brain homogenates, PrP was mostly detected in fractions two to four in an aggregated form (Fig. 3d,i). By contrast, PrP molecules in non-CJD brain samples were detected in fractions six to eight in a monomeric form (Fig. 2b).

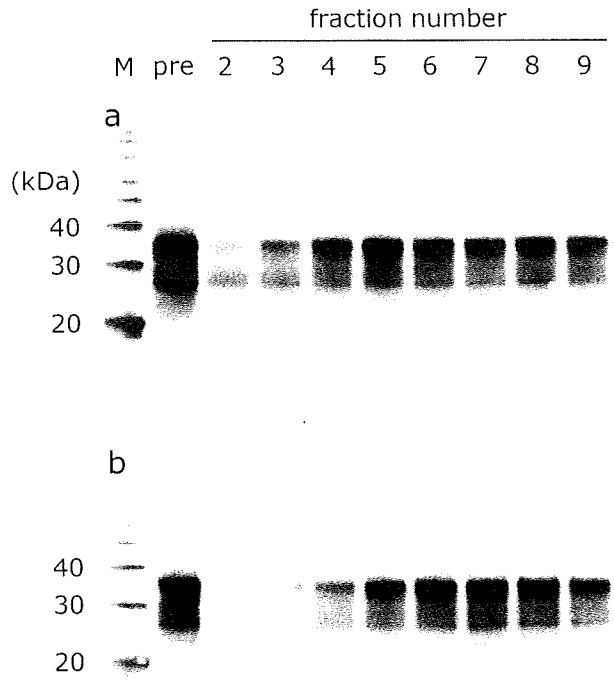

Fig. 2 The effect of buffer conditions on non-CJD homogenate preparation. (a) Samples were prepared in lysis buffer with 0.5% NP-40 and 0.5% deoxycholate, resulting in the detection of PrP molecules in the peak fractions four to six. (b) Most of the PrP molecules were solubilized in the lysis buffer with 1% SDS and shifted into fractions six to eight. pre: Pre-column brain homogenate.

The comparisons of histopathological features between the cases can be seen in Table 1. The findings in the representative cases with short and long disease duration (case 2 and case 5, respectively) can be seen in Figure 3. HE staining (Fig. 3a,f) and GFAP immunostaining (Fig. 3c,h) revealed that spongiosis and gliosis were advanced according to loss of brain weight. All of the CJD cases showed varying degrees of synaptic PrP deposition by PrP immunostaining (Fig. 3b,g). In the case with mild pathological change, PrP molecules were detected as aggregates in fractions two to four, and also as monomers in fractions six to eight (Fig. 3d), whereas in the severe case most of the PrP molecules were aggregated and detected in fractions two to four (Fig. 3i). PrP oligomers retrieved using this method had already developed PK resistance in both the mild and the severe cases (Fig. 3e,j).

The ratio of oligomeric/total PrP was increased according to the disease severity (Fig. 4). PrP oligomers were increased in inverse proportion to the brain weight; however, the ratio plateaued in the very severe cases (cases 1 and 2; Table 1). The increase of PrP oligomers correlated with the grade of histopathological change such as spongiosis and gliosis (Table 1). Moreover, monomeric PrP molecules were consistently decreased in the CJD cases (Fig. 4). The cut-off value of the oligomer ratio was approximately 0.05 between CJD and non-CJD cases.

DISCUSSION

The main difference between the spin-column gel filtration method used in the present study and conventional methods such as western blotting or ELISA is the removal of the protease treatment step. Without protease treatment, protease-sensitive PrP in samples should be retained, and we demonstrated that the PrP molecules can be separated by gel-filtration centrifuge columns using a suitable gel size. The elution curve of each protein was rather broad due to the low resolution of the column; however, the fractionation pattern appeared to be sufficiently effective to distinguish abnormally aggregated PrP oligomers from monomeric PrP^{c} by their size. Fractions two to four contained PrP oligomers of more than 220 kDa, which were discriminated from the monomeric PrP molecules mostly eluted in fractions six to eight. Furthermore, the procedure is safe as the gel filtration method can be performed in a closed system. The CDI method also detects PK-sensitive PrP^{sc} without protease treatment; however this is not based on the polymerization degrees but on the conformational changes of PrP. Therefore, both the gel-filtration method and the CDI method have the advantage of being able to determine PrP^{sc} from different perspectives.

PrP oligomers were increased according to the disease severity in the CJD cases, accompanied by the depletion of

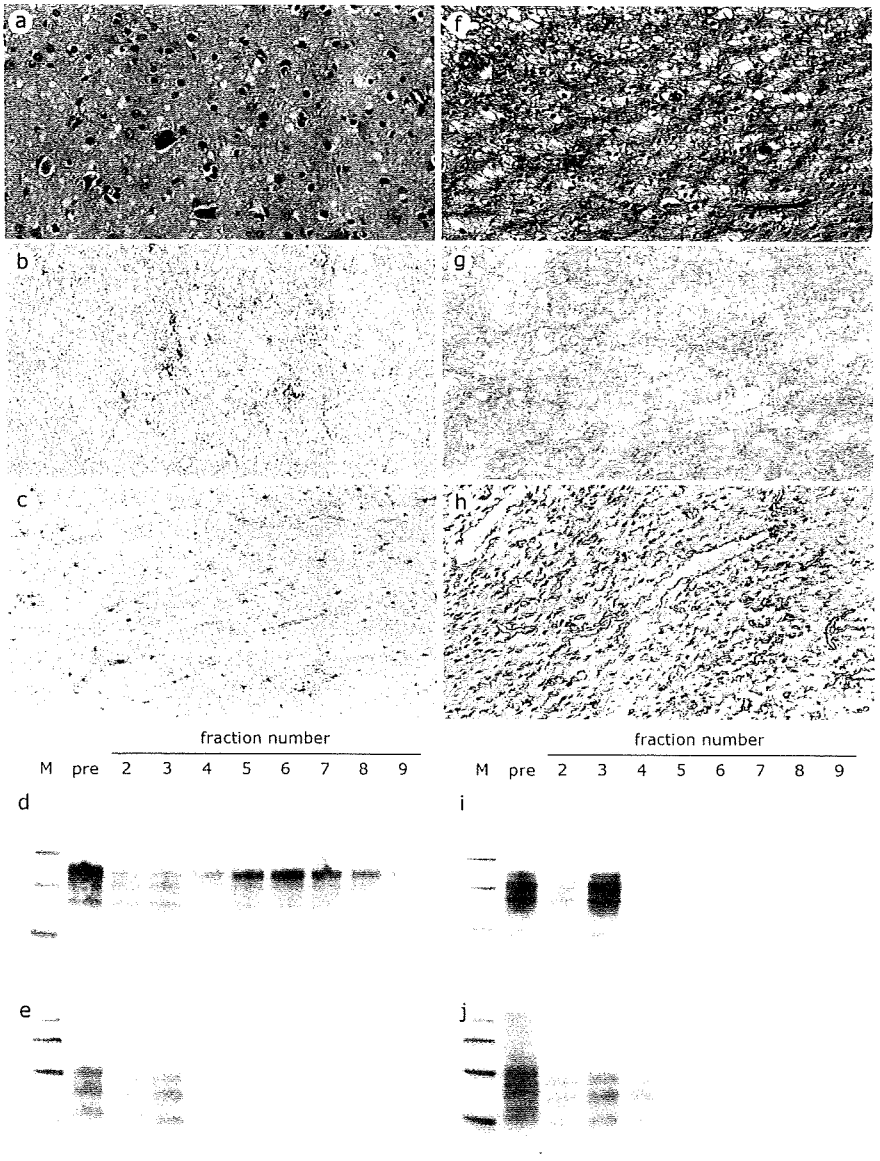

Fig. 3 Comparison of histopathological changes and fractionation patterns of PrP in the CJD cases with short disease duration (case 2 in Table 1, a–e) and long disease duration (case 5, f–i). (a, f) HE staining. (b, g) Immunostaining for PrP. (c, h) GFAP immunostaining. (d, i) Fractionation pattern for PrP. (e, j) Western blot for proteinase-K treated PrP in each fraction. pre: Pre-column brain homogenate. Objective magnification: × 20 (a, f), × 40 (b, g), and × 10 (c, h).

PrP^c. In the cases with short disease duration, CJD-specific pathological changes such as spongiform change, gliosis, and abnormal PrP deposition were less severely observed. PrP oligomers were detected in fractions two to four in those cases, whereas monomeric PrP^c was diminished compared to non-CJD control cases but were still detected in the brain. By contrast, PrP oligomers were more prominent in association with distinctly decreased PrP^c in the cases with long disease duration showing severe rarefaction (status spongiosus) and gliosis in the cerebral cortices. Since human autopsy samples of prion diseases would not exactly correlate with the progression of the disease, a time-course investigation could only be performed using serially collected samples of TSE animal models. However, the relationship of the polymerization degree of PrP to pathological severity such as loss of brain weight, spongiosis and gliosis indicates that dynamic changes of both oligomerization of the human PrP and depletion of normal PrP^c could be responsible for the pathogenesis of human prion diseases.

Previous reports on the polymerization degree of PrP determined by sucrose gradient sedimentation reveal that the PrP monomers and small oligomers are still detected in sporadic CJD samples[9] and prion-infected mouse brains.[10] In this study we demonstrated the almost total depletion of monomeric PrP in some cases with severe pathological changes, which may be due to more intense life-sustaining treatment in our cases. Furthermore, biochemical analyses on animal models would mostly be performed by means of whole brain materials including relatively intact regions,

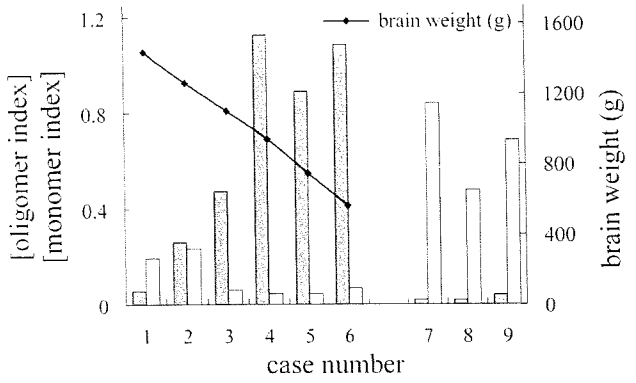

Fig. 4 Correlation between the oligomeric/monomeric PrP and brain weight. Fraction three in this method was supposed to represent the oligomeric PrP and fraction seven corresponded to the monomeric PrP. Pre-column samples were assumed as loading controls of total PrP. The density of triplet PrP bands in each lane was measured, and the oligomeric/total PrP or monomeric/total PrP was calculated as [oligomer index] (gray bars) or [monomer index] (open bars), respectively. The line graph shows the brain weight of CJD cases. The left y-axis shows the index of PrP and the right y-axis shows the brain weight (g).

whereas our biological data in this study were derived exclusively from the relevant lesions. Correlation between the disease progression and the degree of PrP polymerization requires further elucidation by analyses of larger-scale samples including serially collected samples of TSE animal models and human TSE cases with different clinicopathological features such as prion protein gene codon 129 genotypes, PrP^{sc} isoforms and PrP deposition pattern.

Although PrP oligomers were increased according to the disease stages, the ratio of oligomeric/total PrP plateaued in the very severe case. It must be noted that the uppermost limit of the size of the retrieved proteins using this method is unknown, and highly aggregated PrP fibrils may remain stuck in the gel bed. It is possible that abnormal PrP molecules would mostly form amyloid fibrils with a long disease duration, which could not be retrieved using this method. Sucrose gradient sedimentation was previously shown to detect all the detergent-insoluble PrP aggregates,[9,10] including amyloid fibrils, but the gel-filtration column method used in the present study is a suitable and more convenient method for retrieval of PrP oligomers.

In conclusion, the simplified gel-filtration method can detect PrP oligomers in human CJD cases. This method would detect not only PK-resistant PrP^{res}, but also PK-sensitive PrP^{sc}. The increase of PrP oligomers correlated with the degree of brain pathology such as spongiosis and gliosis. Further studies are required to confirm the biochemical characteristics of these oligomers, including the measurement of polymerization degree of PrP detected in fractions two to four, and whether these fractions are neurotoxic and/or infectious.

ACKNOWLEDGMENTS

This work was supported by grants to K. Sasaki from the Ministry of Health, Labour and Welfare, Japan (H19-nanchi-ippan-006) and the Japan Society for the Promotion of Science (No. 19500309). The authors thank Ms. S. Nagae and Ms. K. Sato for their technical support.

REFERENCES

1. Creutzfeldt HG. On a particular focal disease of the central nervous system (preliminary communication), 1920. *Alzheimer Dis Assoc Disord* 1989; **3**: 3–25.
2. Prusiner SB. Prions. *Proc Natl Acad Sci USA* 1998; **95**: 13363–13383.
3. Thackray AM, Hopkins L, Bujdoso R. Proteinase K-sensitive disease-associated ovine prion protein revealed by conformation-dependent immunoassay. *Biochem J* 2007; **401**: 475–483.
4. Safar J, Wille H, Itri V *et al.* Eight prion strains have PrP^{Sc} molecules with different conformations. *Nat Med* 1998; **4**: 1157–1165.
5. Tremblay P, Ball HL, Kaneko K *et al.* Mutant PrP^{Sc} conformers induced by a synthetic peptide and several prion strains. *J Virol* 2004; **78**: 2088–2099.
6. Safar JG, Geschwind MD, Deering C *et al.* Diagnosis of human prion disease. *Proc Natl Acad Sci USA* 2005; **102**: 3501–3506.
7. Caughey B, Lansbury PT. Protofibrils, pores, fibrils, and neurodegeneration: separating the responsible protein aggregates from the innocent bystanders. *Annu Rev Neurosci* 2003; **26**: 267–298.
8. Silveira JR, Raymond GJ, Hughson AG *et al.* The most infectious prion protein particles. *Nature* 2005; **437**: 257–261.
9. Yuan J, Xiao X, McGeehan J *et al.* Insoluble aggregates and protease-resistant conformers of prion protein in uninfected human brains. *J Biol Chem* 2006; **281**: 34848–34858.
10. Pan T, Wong P, Chang B *et al.* Biochemical fingerprints of prion infection: accumulations of aberrant full-length and N-terminally truncated PrP species are common features in mouse prion disease. *J Virol* 2005; **79**: 934–943.
11. Sharon R, Bar-Joseph I, Frosch MP, Walsh DM, Hamilton JA, Selkoe DJ. The formation of highly soluble oligomers of α-synuclein is regulated by fatty acids and enhanced in Parkinson's disease. *Neuron* 2003; **37**: 583–595.

12. Singer SJ, Dewji NN. Evidence that Perutz's double-β-stranded subunit structure for β-amyloids also applies to their channel-forming structures in membranes. *Proc Natl Acad Sci USA* 2006; **103**: 1546–1550.
13. Lue LF, Kuo YM, Roher AE *et al.* Soluble amyloid β peptide concentration as a predictor of synaptic change in Alzheimer's disease. *Am J Pathol* 1999; **155**: 853–862.
14. Walsh DM, Klyubin I, Fadeeva JV, Rowan MJ, Selkoe DJ. Amyloid-β oligomers: their production, toxicity and therapeutic inhibition. *Biochem Soc Trans* 2002; **30**: 552–557.
15. Dahlgren KN, Manelli AM, Stine WB *et al.* Oligomeric and fibrillar species of amyloid-β peptides differentially affect neuronal viability. *J Biol Chem* 2002; **277**: 32046–32053.
16. Kayed R, Head E, Thompson JL *et al.* Common structure of soluble amyloid oligomers implies common mechanism of pathogenesis. *Science* 2003; **300**: 486–489.
17. Lambert MP, Barlow AK, Chromy BA *et al.* Diffusible, nonfibrillar ligands derived from Aβ1-42 are potent central nervous system neurotoxins. *Proc Natl Acad Sci USA* 1998; **95**: 6448–6453.
18. Notari S, Capellari S, Giese A *et al.* Effects of different experimental conditions on the PrP^{Sc} core generated by protease digestion: implications for strain typing and molecular classification of CJD. *J Biol Chem* 2004; **279**: 16797–16804.

Journal of Pathology
J Pathol 2009; **219**: 123–130
Published online 11 May 2009 in Wiley InterScience
(www.interscience.wiley.com) **DOI:** 10.1002/path.2576

Original Paper

Development of oligomeric prion-protein aggregates in a mouse model of prion disease

Kensuke Sasaki,* Haruhiko Minaki and Toru Iwaki
Department of Neuropathology, Neurological Institute, Graduate School of Medical Sciences, Kyushu University, Fukuoka, Japan

*Correspondence to:
Kensuke Sasaki, Department of Neuropathology, Neurological Institute, Graduate School of Medical Sciences, Kyushu University, Fukuoka 812-8582, Japan.
E-mail:
ksasaki@np.med.kyushu-u.ac.jp

No conflicts of interest were declared.

Abstract

In prion diseases the normal cellular isoform of prion protein (PrP), denoted PrP^{C}, is converted into an abnormal, pathogenic isoform of PrP (PrP^{Sc}). Diagnostic tools for prion diseases are conventionally based on the detection of protease-resistant PrP (PrP^{res}) after proteinase K digestion. However, recent studies have revealed that protease-sensitive abnormal PrP ($sPrP^{Sc}$) also exists in significant amounts in brains suffering from prion diseases. Here, we designed a simplified size-exclusion gel chromatography assay, using disposable spin columns to examine PrP aggregates in the course of the disease, without proteinase K digestion. Brain homogenates of NZW mice, inoculated intracranially with Fukuoka-1 strain, and which died at around 120 days post-inoculation, were assayed by this gel-fractionation method and eluted PrP molecules in each fraction were detected by western blot analysis. Oligomeric PrP molecules were well separated from monomers, as predicted. A conventional protease-digestion assay was also performed to detect PrP^{res} and revealed that the ratio of PrP^{res} to total PrP increased drastically from 105 days. However, the increase of PrP oligomers became significant from 90 days. These PrP oligomers in the early disease stage would, therefore, be $sPrP^{Sc}$ molecules that might affect the disease pathology, such as spongiform change and abnormal PrP deposition. We also observed that the resistance of PrP oligomers to proteinase K and insolubility in phosphotungstic acid precipitation increased with disease progression, which suggests that PrP oligomers are not clearly distinguished from cellular PrP or PrP^{res} but may overlap in a continuous spectrum. Our study casts light on the ambiguity of the definition of PrP^{Sc} and indicates that the abnormality of PrP molecules should be determined from various perspectives, more than protease resistance.

Received: 13 February 2009
Revised: 31 March 2009
Accepted: 5 May 2009

Keywords: prion; oligomer; transimissible spongiform encephalopathy; Creutzfeldt–Jakob disease; mouse model

Introduction

Transmissible spongiform encephalopathies (TSEs), also termed prion diseases, are fatal neurodegenerative diseases associated with abnormal deposition of prion protein (PrP) in the central nervous system. The normal cellular isoform of PrP, denoted PrP^{C}, is converted into an abnormal, protease-resistant, pathogenic isoform of PrP (PrP^{Sc}) by post-translational modification. The conversion of PrP^{C} into PrP^{Sc} involves a conformational change of the protein, from an α-helical to a β-sheet structure, and PrP^{Sc} forms detergent-insoluble aggregates and is partially resistant to proteinase K (PK) digestion [1]. Conventional diagnostic tools for prion diseases are based on the detection of protease-resistant abnormal PrP (PrP^{res} or $rPrP^{Sc}$) after PK digestion. However, recent studies have revealed that protease-sensitive abnormal PrP ($sPrP^{Sc}$) also exists at significant levels in TSE brains [2–5]. Due to the avoidance of protease digestion, conformation-dependant immunoassay (CDI) has been recently developed to detect total PrP^{Sc}, including $sPrP^{Sc}$ [3–7]. Other novel methods for the detection of PrP^{Sc} that do not require protease treatment have also been developed, such as sucrose gradient sedimentation and size-exclusion gel chromatography to detect abnormally aggregated PrP [8,9], fluorescence-based conformational biosensor to detect β-folded conformation of PrP [10], fluorescence correlation spectroscopy to detect prion particles [11] or modified sandwich ELISA to detect PrP oligomers [12].

It is well established that in many neurodegenerative diseases, designated as 'conformational diseases', the oligomeric form of disease-causing protein is more lethally neurotoxic than the highly aggregated fibrillar form. Amyloid β protein in Alzheimer's disease [13,14], α-synuclein in Lewy body disease [15] and polyglutamine protein in polyglutamine diseases

[16] form pathogenic oligomers that give rise to channel-forming structures, which lead to inappropriate membrane permeabilization [17,18]. In this context, protein aggregation into amyloid fibrils might be a protective process for the nervous system [19]. PrP^{Sc} also aggregates into oligomers or fibrils, whose minimal structures have recently been modelled as β-helical PrP trimers [20,21] reminiscent of channel-forming structures. Thus, toxic PrP peptide could form ion-permeable channels in lipid bilayer membranes [22]. Indeed, recent studies have indicated that PrP oligomers have more intense infectivity [23] and neurotoxicity [24,25] than highly aggregated amyloid fibrils, which corresponds to soluble amyloid β oligomers in Alzheimer's disease [13,14].

To explore the PrP molecules with intermediate properties between PrP^{C} and PrP^{res}, such as $sPrP^{Sc}$ or PrP oligomers, we developed a simplified size-exclusion gel chromatography assay using disposable gel-filtration spin columns. This method provides a tool for measuring the aggregation status of total PrP without PK digestion and to detect PrP oligomers in an easy and safe way. We employed this method to examine the time course for the development of PrP aggregates in a TSE mouse model. We also determined the characteristics of detected PrP oligomers to evaluate their association with disease progression.

Materials and methods

TSE mouse model

NZW mice were inoculated intracranially with the mouse-adopted Fukuoka-1 strain derived from a human case with Gerstmann–Sträussler–Scheinker disease [26]. Brain samples were serially collected twice a month until the mice died at around 120 days post-inoculation. At each time point, three brains were fixed in 10% formalin for pathological examination and three to four brains were frozen together in a single test tube for biochemical analyses. Control samples were also collected from the mock-treated mice, which had been inoculated with normal brain homogenate. Formalin-fixed, paraffin-embedded sections were stained with haematoxylin and eosin (H&E) to examine spongiform change, neuronal loss and gliosis. Spongiform change was assessed by image-analysis software (ImageJ, National Institutes of Health, USA), in which the highlighted area of vacuoles was calculated and divided by the total area, designated as a spongiform index [vacuolar/total area (%)]. Data were compared between groups at each time point using Tukey's test. Immunohistochemistry for PrP was performed using a polyclonal anti PrP C-terminal antibody (1 : 200; IBL, Japan) in conjunction with the detergent autoclaving method for antigen retrieval [27]. The procedures performed in this study were approved by the Committee of Ethics on Animal Experiments of the Faculty of Medicine, Kyushu University, and were in strict accordance with the Guidelines for Animal Experiments of the Faculty of Medicine, Kyushu University, and with Law No. 105 and Notification No. 6 of the Japanese Government.

Detection of PrP^{res}

Conventional procedures for the detection of PrP^{res} were conducted as follows: 1% brain homogenate was prepared in extraction buffer (100 mM Tris–HCl, 100 mM NaCl, 10 mM EDTA, 0.5% Nonidet P-40, 0.5% sodium deoxycholate, pH 7.6) and incubated with 50 μg/ml PK at 37 °C for 1 h. Protease activity was then abolished by the addition of 1 mM Pefabloc SC (Roche, USA). Undigested PrP^{res} fragments were separated by SDS–polyacrylamide gel electrophoresis (SDS–PAGE) in 12% NuPAGE Bis–Tris gels (Invitrogen, USA) and transferred onto polyvinilidene difluoride membranes (Millipore, USA). Protein was detected using anti-PrP mAb (clone SAF-83, raised against scrapie-associated fibrils from infected hamster brain, 1 : 10 000; Cayman, USA) as the primary antibody and peroxidase-labelled donkey anti-mouse IgG Ab (AP192P, 1 : 20 000; Chemicon, USA) as the secondary antibody, and visualized by chemiluminescence with ECL-plus substrate (GE Healthcare, UK). Another anti-PrP SAF-70 mAb (Cayman) recognizing amino acid residues 142–160 was also used to determine the specificity.

Spin-column gel filtration

We tested the spin-column kit CHROMA SPIN-200 (Clontech, USA) for its ability to fractionate proteins according to molecular size. The manufacturer's instructions refer to the size-selective separation and purification of nucleic acids, which indicate the capability to retrieve nucleic acids of >350 bases and eliminate proteins <1000 kDa; thus, we had to modify the procedures to enable the fractionation of proteins. Briefly, low-speed centrifugation following additional loads of extraction buffer were repeated to collect size-selected fractions. The modified protocol is summarized in Figure 1A. Columns were pre-spun at $200 \times g$ for 3 min to remove storage buffer. Buffer exchange was made by the addition of 500 μl extraction buffer followed by centrifugation at $200 \times g$ for 3 min. This step was then repeated. For easier sample loading, 0.01% bromophenol blue was added to 1% brain homogenates and then 75 μl sample was applied on the gel bed. Elution fractions were gathered into collection tubes by spinning at $120 \times g$ for 2 min. Fractions were serially collected by repeated addition of 40 μl extraction buffer followed by centrifugation. Fractionated PrP was detected without PK treatment by SDS–PAGE and western blot analysis, as described above.

To evaluate fractionation profiles produced by this method, we applied western protein standards, MagicMark XP (Invitrogen, USA), to a spin column. Marker

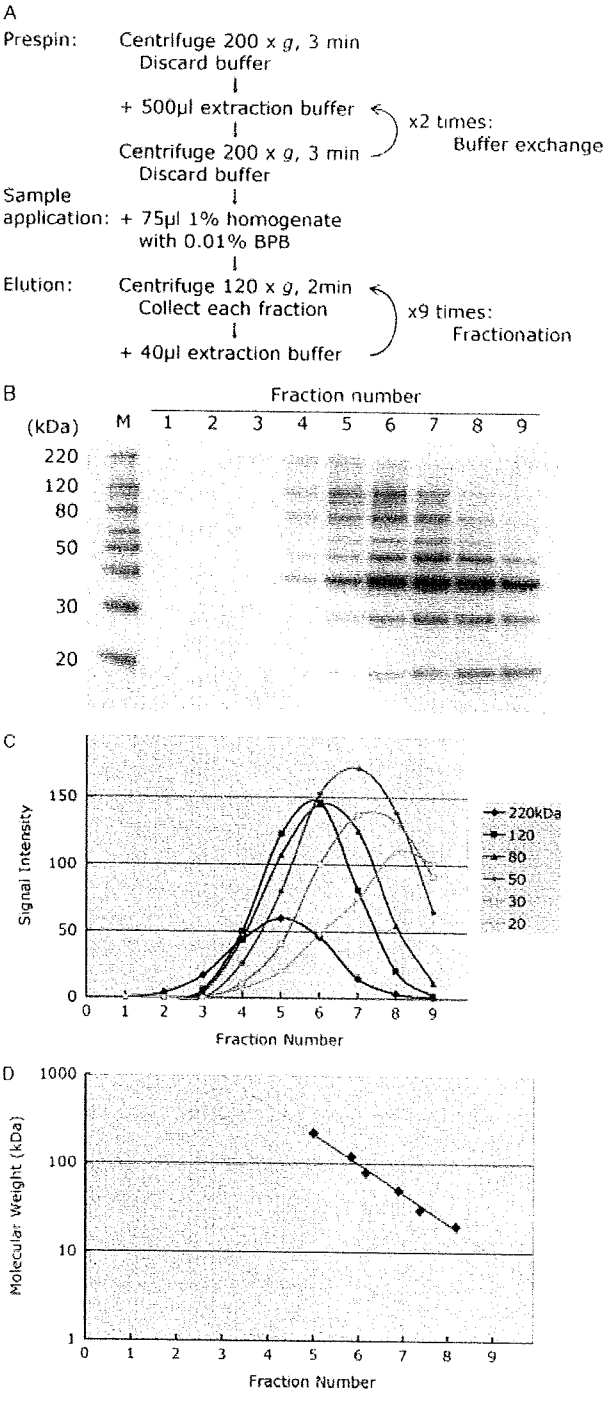

Figure 1. The fractionation capability of spin columns. (A) Protocol for the spin-column gel filtration method. CHROMA SPIN TE-200 (Clontech) columns were used. BPB, bromophenol blue. (B–D) Molecular-weight markers [MagicMark XP, Invitrogen; lane M in (B)] were gel-fractionated. The marker molecules eluted in each fraction were evaluated by SDS–PAGE (B) and a chromatogram was obtained from grey value measurements (C). Peak fractions of each molecule were estimated and plotted against molecular weight (kDa) (D). A log-linear relation was observed among 20–220 kDa molecules

proteins were prepared in sample buffer (NuPAGE LDS sample buffer; Invitrogen), to mimic the molecular size in the condition of SDS–PAGE, and fractionated by the spin-column gel filtration method. Each fraction was assessed by western blot analysis, as described above.

Biochemistry of fractionated PrP

PrP molecules in each fraction prepared by the gel-filtration method were examined for protease resistance using 50 µg/ml PK treatment to detect PrP^{res}, as described above. Phosphotungstic acid (PTA) precipitation was also conducted on each fraction, without PK treatment, to estimate the total disease-associated PrP^{Sc}, as described previously [28] except avoiding the enrichment effect. Specifically, 10 µl fractions were treated with PTA and the resulting pellets were resuspended in 10 µl sample-loading buffer. Prepared PrP molecules were detected by western blot analysis, as described above. Deglycosylation by PNGase F (peptide-N-glycosidase F; New England Biolabs, USA) was also performed in accordance with the manufacturer's instructions to determine the PrP fragments unambiguously.

To determine whether fractionated PrP molecules have the form of oligomers, dot-blot analysis was performed using 2 µl each fraction dotted onto a nitrocellulose membrane. Oligomers were detected using a primary anti-oligomer antibody [29] (rabbit polyclonal A11, 1 : 5000, Invitrogen, USA) and peroxidase-labelled donkey anti-rabbit IgG Ab (AP187P, 1 : 10 000, Chemicon, USA) as the secondary antibody. The oligomer-specific immunoreaction was detected by a chemiluminescent assay.

Results

Fractionation capability of spin columns

The fractionation pattern of molecular weight markers, as shown in Figure 1B–D, indicated that the elution curve of each marker protein was rather broad, due to the low resolution of the column; however, the fractionation pattern appeared to be sufficiently effective to distinguish, by size, abnormally aggregated PrP oligomers from monomer PrP^{C}. Although fraction 1 consisted mostly of the void volume and contained insufficient protein to be assessed, the size of eluted protein molecules in fractions 2 and 3 was estimated to be >200 kDa in reference to the chromatogram and the standard curve of peak fractions (Figure 1C, D). Proteins whose molecular weights were approximately 30 kDa, such as monomer PrP molecules, were collected mainly in fractions 6–8.

Profiles of the NZW/Fukuoka-1 mouse model

NZW mice, inoculated intracranially with Fukuoka-1 strain, died approximately 120 days post-inoculation. Spongiform change in the thalamus was specifically prominent from 90 days (Figure 2A–C), while fine vacuolation and gliotic change in the cerebral cortex

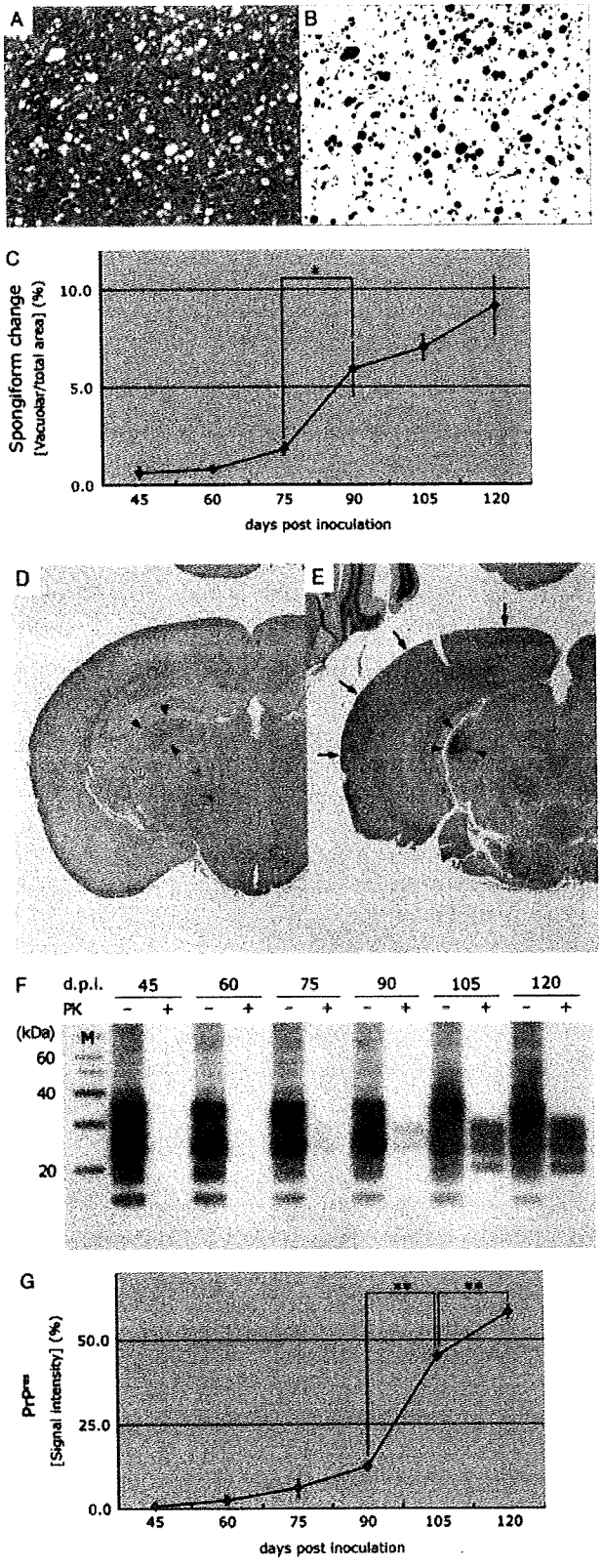

was observed from 105 days (data not shown). Abnormal PrP deposition, predominantly observed in a punctate synaptic pattern, was first detected by immunohistochemistry from 60 days in the lateral thalamic nucleus (Figure 2D, arrow heads), which became more intense with time (Figure 2E, arrow heads) and spread into the cerebral cortex from 105 days (Figure 2E, arrows). Even though PrP^{res} was already detected in 90 day samples, the ratio of PrP^{res} to total PrP increased significantly from 105 days (Figure 2F, G), which corresponded to the time course of abnormal PrP deposition spreading throughout the brain, including to the cerebral cortex.

Time course of the development of PrP aggregates

The spin-column gel filtration method revealed that PrP aggregates increased with respect to disease progression, and that the development of PrP oligomers preceded the appearance of PrP^{res}. Most of the PrP molecules extracted from the control and 45 day samples were monomers that were collected mainly in fractions 6–8 (Figure 3A, B). Meanwhile, PrP aggregates collected in fractions 2–4 were significantly increased from 90 days (Figure 3B, and the time-course chart shown in Figure 3C), which preceded the augmentation of PrP^{res} from 105 days. In the early disease stage, fractionated PrP aggregates at 90 days were not effectively retrieved by PTA precipitation (Figure 4A), although these molecules were certainly in the form of oligomers, as indicated by the dot-blot analysis with anti-oligomer antibody (Figure 4B). In the terminal disease stage, fractionated PrP oligomers at 120 days acquired an unexpectedly high level of PK resistance (Figure 5B) and were precipitated in conjunction with PTA, even though the retrieved PrP molecules were apparently less than those in original fractions (Figure 5C).

Time course of the modification of PrP fragments

PNGase deglycosylation elucidated that total PrP consisted of full-length molecules and smaller fragments other than PrP^{res} (Figure 6), possibly derived from endogenous proteolytic cleavage [30], which caused complicated band patterns in western blot analyses. Anti-PrP SAF-70 mAb, which recognizes amino acid residues 142–160, also detected a similar fragment

Figure 2. Profiles of the NZW/Fukuoka-1 mouse model. (A–C) Assessment of the spongiform change in the lateral thalamic region. Coarse or fine vacuoles were specifically observed at 120 days post-inoculation. (A; H&E, magnification ×200). The area of vacuoles was highlighted (B) and calculated as the spongiform index [vacuolar/total area (%)] at each time point (C). Spongiform change in the thalamus was significantly exacerbated from 90 days ($^{*}p = 0.0011$, Tukey's test; three mice were examined at each point). (D, E) Time course of PrP deposition (immunohistochemistry for PrP, magnification ×12.5). Representative sections prepared at 60 (D) and 105 days (E) are shown. Punctate synaptic deposition of PrP was observed in the thalamus (arrowheads) and the cerebral cortex (arrows). (F, G) Development of PrP^{res}. The signal intensity index was calculated as the percentage of the density of PK-resistant PrP against total PrP without PK treatment (G). The ratio of PrP^{res} was drastically increased from 105 days ($^{**}p < 0.0001$, Tukey's test; experiments were performed in triplicate). PK, proteinase-K treatment; M, molecular weight markers

J Pathol 2009; **219**: 123–130 DOI: 10.1002/path

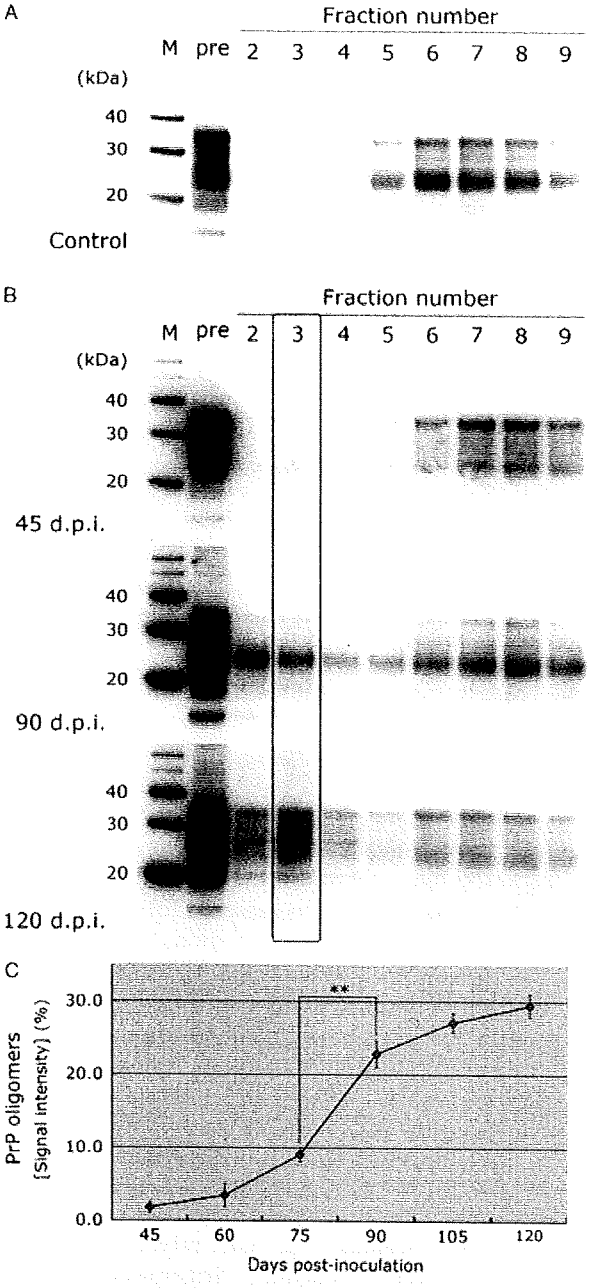

Figure 3. The development of PrP aggregates precedes the appearance of PrP^{res} molecules. (A, B) The PrP molecules in 1% brain homogenates were fractionated by spin-columns and detected by western blot analysis. Representative results of the control sample collected at 120 days post mock-inoculation (A), and the diseased samples at 45, 90 and 120 days post-inoculation (d.p.i.) (B) are shown. (C) The signal intensity index of PrP oligomers [fraction 3 in (B)] was calculated as the percentage against total PrP [pre in (B)]. PrP aggregates were significantly increased from 90 days (**$p < 0.0001$, Tukey's test; experiments were performed in triplicate). M, molecular weight markers; pre, unfractionated 1% brain homogenates were loaded to provide the index of total PrP

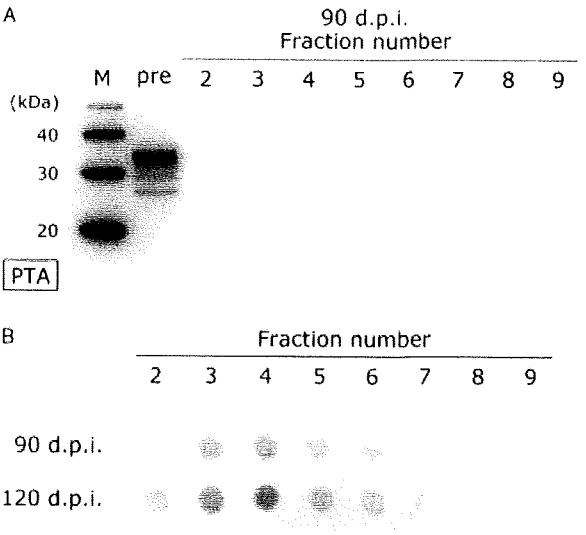

Figure 4. Characteristics of PrP oligomers at the early disease stage. (A) The sample at 90 days post-inoculation (d.p.i.) was fractionated and PTA precipitation was conducted for the same amount of each fraction applied in Figure 3B. No aggregated PrP molecule was precipitated in fractions 2 and 3, neither were monomers detected (fractions 7 and 8). Note that retrieved PrP molecules from the unfractionated sample (pre) were also far less than those in the original sample shown in Figure 3B. (B) Fractionated PrP aggregates were certainly oligomer molecules. Anti-oligomer antibody (Invitrogen) detected PrP oligomers at 90 and 120 days by dot-blot immunoassay. PrP molecules in fractions 8 and 9 should be mostly monomers, which can be considered as negative controls. PTA, phosphotungstic acid precipitation; M, molecular weight markers; pre, unfractionated 1% brain homogenate

pattern (data not shown). PK-sensitive PrP in the control and also PrP oligomers in the early disease stage showed a prominent diglycosylated form, of both full-length and endogenously truncated fragments (Figures 3A, B, 6), whereas PrP^{res} in the terminal stage showed almost even quantities of three glycoform bands, of both full-length and PK-digested fragments (Figures 5B, C, 6). Monomeric PrP in the terminal stage was indeed PK-sensitive and PTA-soluble, and still retained the prominent diglycosylated pattern (Figure 5A). PrP oligomers in the terminal stage also involved the PrP^{res}-like fragments, which would be digested by endogenous proteases reminiscent of PK (Figures 5A, 6).

Discussion

The spin-column gel filtration method was simple yet effective for the separation of PrP aggregates and monomeric PrP^{C}. The method was confined to a closed system, contributing to safe handling. Elution curves were rather broad, due to the low resolution of the column; however, monomer PrP molecules, retrieved mainly in fractions 6–8, were well demarcated from oligomers in fractions 2–4, in accordance with our expectations. The reproducibility of the technique was confirmed, as shown in Figure 3B, in which standard deviations of the data at each time point were sufficiently small to compare each group statistically. The peak fraction of oligomers detected by dot-blot was found in fraction 4, which was slightly later